



Interaction Between Tollmien-Schlichting Waves And Free-Stream Disturbances In Boundary-Layer Flows

R. J. Bodonyi
Department of Aeronautical and Astronautical Engineering

National Aeronautics and Space Administration
Lewis Research Center
Cleveland, Ohio 44135

Grant No. NAG 3-743
Final Report
RF Project 765803/719039

August 1989

TABLE OF CONTENTS

Preface	iii
Summary	iv
Introduction	1
Problem Formulation	4
Numerical Method	
Steady-state Solution	11
Unsteady Solution	12
Numerical Results	16
Acknowledgement	25
References	26
Figures	28

PREFACE

The work described in this report was carried out under NASA Grant No. NAG 3-743 "Interaction Between Tollmien-Schlichting Waves and Free-stream Disturbances in Boundary-layer flows". The program was monitored by Dr. M.E. Goldstein, Office of the Chief Scientist, NASA Lewis Research Center. The principal investigator was Professor Richard J. Bodonyi, Department of Aeronautical and Astronautical Engineering, The Ohio State University. The results of this study will appear in a paper co-authored with J.W.C. Welch, P.W. Duck and M. Tadjfar in the Journal of Fluid Mechanics. This report constitutes the final technical report for this project.

SUMMARY

A numerical study of the generation of Tollmien-Schlichting waves due to the interaction between a small freestream disturbance and a small localized variation of the surface geometry has been carried out using finite difference methods. The nonlinear steady flow is of the viscous-inviscid interactive type while the unsteady disturbed flow is assumed to be governed by the Navier-Stokes equations linearized about this flow. Numerical solutions illustrate the growth or decay of the T-S waves generated by the interaction between the freestream disturbance and the surface distortion, depending on the value of the scaled Strouhal number. An important result of this receptivity problem is the numerical determination of the amplitude of the Tollmien-Schlichting waves.

1. Introduction

The steady and unsteady effects of small surface-mounted obstacles on the boundary-layer flow over a surface have been of concern for many years. These effects include most notably separation and instability, often leading to transition to turbulence. Two main reasons possible for this transition have been suggested: either the surface distortion produces, in effect, a locally separated shear flow which is susceptible to inviscid instabilities associated with the inflectional velocity profile [see Smith & Bodonyi 1982, 1985, 1987 and Bodonyi, Smith & Gajjar 1983 for a discussion of these inviscid type instabilities], or there is a sensitive interaction between the surface distortion and the basic flow, possibly with unsteadiness/turbulence in the free stream, which can readily accentuate the viscous-inviscid growth of the Tollmien-Schlichting instabilities usually present in boundary layers in any case.

The major steady-flow phenomenon observed, separation, is now well understood, at least in two-dimensional flows. It is generally of an interactive viscous-inviscid type in which the flows inside and outside the boundary layer affect each other significantly within a relatively short length scale. The question of the stability of the separating flow or other locally distorted steady or unsteady motions is always present, however, and this has started to receive increased

attention, in part because of modern developments in boundary-layer methods.

In this study our concern is with the possibility of the generation of Tollmien-Schlichting (T-S) waves due to the interaction of small free-stream disturbances and localized variations in the surface geometry. In general terms, the sequence of events that begins with the excitation of spatially growing T-S waves in a boundary layer by free-stream disturbances is known as the receptivity problem [Morkovin 1969]. It has been studied by a number of authors over the years and the area has been reviewed by Reshotko (1976). More recently, Murdock (1980), Goldstein (1983, 1984, 1985), Goldstein, Sockol & Sanz (1983) and Goldstein, Leib & Cowley (1987) have theoretically investigated the role that small free-stream disturbances play in generating T-S waves in boundary-layer flows in a variety of situations. In particular we note that Goldstein (1985) studied the effect that small variations in surface geometry have on scattering weak unsteady free-stream disturbances into Tollmien-Schlichting waves. Using the triple-deck scalings of Stewartson (1969), Goldstein concluded that relatively small surface variations which provoke correspondingly small pressure changes can produce a large coupling between the T-S waves and the imposed disturbance when these variations are sufficiently rapid, i.e., when they occur on the scale of a T-S wave. Goldstein's analysis provided a qualitative explanation of the Leehey & Shapiro (1979) boundary-layer receptivity measurements. Further comparisons with the Leehey & Shapiro

experiments using a solution of the local Orr-Sommerfeld equation have been made by Goldstein & Hultgren (1987).

However, Goldstein's analysis is limited in that he took for the steady flow the linearized solution of Stewartson (1970, 1971) for the interactive flow in the vicinity of a sharp corner in an incompressible flow. Thus Goldstein could not consider the effects of surface variations of sufficient size to provoke boundary-layer separation or even a nonlinear response in the steady flow, although his analysis does account for nonparallel flow effects on the stability of the flow.

Since our interest is in the stability of nonparallel flows and especially those with strong local streamwise variations in surface geometry, it is appropriate to take the steady nonlinear viscous-inviscid interactive solutions, of the triple-deck and similar kinds, for the basic steady motion. This is because, as is now well-known, flow reversal for small or large scale separations occurring in such flows is not necessarily a catastrophic event: the solution at the separation point is regular due to the presence of interaction, unlike that in steady classical, i.e. noninteractive, boundary layers for instance. Hence a steady nonparallel basic flow with a small localized region of reversed flow can be described fully by the classical boundary-layer equations, subject to an unknown pressure which must also be computed as part of the solution. Additionally, we shall assume that the unsteady flow is governed by the linearized Navier-Stokes equations, as discussed in the following section.

2. Problem Formulation

We wish to study the interaction between an unsteady freestream and a small surface perturbation on a flat plate, such as a hump or trough, for an incompressible two-dimensional viscous flow. Thus following Goldstein (1985) we take the upstream motion to consist of a uniform flow with velocity U_∞^* plus a small harmonic perturbation of frequency Ω and constant amplitude $u_\infty^* \ll U_\infty^*$, so that the unsteady motion can be analyzed as a linear perturbation of the uniform steady flow, U_∞^* , i.e., $U_\infty^*(1 + u_\infty^*/U_\infty^* e^{-i\Omega t^*})$.

Consider a Cartesian coordinate system (x^*, y^*) with x^* tangent to and y^* normal to the flat plate with the origin taken at the leading edge. Further, define the Reynolds number $Re = U_\infty^* L^* / \nu$, where L^* is the distance of the surface perturbation from the leading edge of the flat plate and ν is the kinematic viscosity of the fluid. For convenience, we introduce the small parameter $\epsilon = Re^{-1/8}$ and consider solutions of the Navier-Stokes equations when $Re \gg 1$. Specifically, we wish to consider the problem of flow over a small hump of length $O(L^* \epsilon^3)$ and height $O(L^* \epsilon^5)$ with a profile of the form

$$y^*/L^* = \epsilon^5 F((x^* - L^*)/\epsilon^3 L^*) , \quad (2.1)$$

with $F = O(1)$, positioned at a distance L^* from the leading edge. The interaction region is shown schematically in Figure 1.

Following Goldstein (1985) we write

$$\hat{U}(x, y, t) = U_0(x, y) + \delta \bar{u}(x, y, t) , \quad (2.2)$$

$$\hat{V}(x, y, t) = V_0(x, y) + \delta \bar{v}(x, y, t) , \quad (2.3)$$

$$\hat{P}(x, y, t) = P_0(x, y) + \delta \bar{p}(x, y, t) , \quad (2.4)$$

where the steady velocity components, U_0 , V_0 , and pressure, P_0 , are normalized by U_∞^* and ρU_∞^{*2} , respectively and $\bar{u}, \bar{v}, \bar{p}$ the unsteady velocity and pressure terms normalized by u_∞^* and $\rho u_\infty^* U_\infty^*$, respectively. Furthermore, we define

$$x = (x^* - L^*)/L^*, \quad y = y^*/L^*, \quad t = \Omega t^*, \quad \delta = u_\infty^*/U_\infty^*. \quad (2.5)$$

Substituting (2.2) - (2.4) into the Navier-Stokes equations and neglecting terms of $O(\delta^2)$, we get the linearized perturbation equations

$$S\bar{u}_t + U_0\bar{u}_x + \bar{u}U_{0x} + V_0\bar{u}_y + \bar{v}U_{0y} = -\bar{p}_x + Re^{-1}[\bar{u}_{xx} + \bar{u}_{yy}], \quad (2.6)$$

$$S\bar{v}_t + U_0\bar{v}_x + \bar{u}V_{0x} + V_0\bar{v}_y + \bar{v}V_{0y} = -\bar{p}_y + Re^{-1}[\bar{v}_{xx} + \bar{v}_{yy}], \quad (2.7)$$

$$\bar{u}_x + \bar{v}_y = 0, \quad (2.8)$$

where $S = \Omega L^*/U_\infty^*$, (2.9)

is the Strouhal number.

Finally, we note that the physical interaction between the oncoming boundary layer, freestream disturbance, and hump is governed by a triple-deck structure, centered near the surface distortion. The details of the structure as applied to this problem have been given by Goldstein (1985) and we, therefore, only summarize the relevant portions here. As is usually the case the viscous interaction problem essentially reduces to a study of the lower-deck equations. Thus the appropriately scaled variables in the lower deck for the steady flow are

$$U_0(x, y) = \epsilon U(X, Y) + O(\epsilon^2), \quad (2.10)$$

$$V_0(x, y) = \epsilon^3 V(X, Y) + O(\epsilon^4), \quad (2.11)$$

$$P_0(x, y) = \epsilon^2 P(X) + O(\epsilon^3), \quad (2.12)$$

where $X = x/\epsilon^3$, $Y = y/\epsilon^5$. (2.13)

U, V, and P are found from the solution of the lower-deck equations:

$$U_X + V_Y = 0, \quad (2.14)$$

$$UU_X + VU_Y = -P_X + U_{YY}, \quad (2.15)$$

subject to the boundary conditions

$$U = V = 0 \quad \text{on } Y = F(X), \quad (2.16)$$

$$(U, V, P) \rightarrow (Y, 0, 0) \quad \text{as } |X| \rightarrow \infty, \quad (2.17)$$

$$U \rightarrow [Y + A(X)], \quad Y \rightarrow \infty, \quad \text{all } X, \quad (2.18)$$

where we have assumed that a simple renormalization of the variables has been carried out in order to set the value of the wall shear of the oncoming, undisturbed boundary layer to unity.

Finally, the interaction condition for incompressible flow is given by the Cauchy Hilbert integral

$$P(X) = 1/\pi \int_{-\infty}^{\infty} (X-\xi)^{-1} (dA/d\xi) d\xi. \quad (2.19)$$

This steady problem was originally formulated by Smith (1973).

For the unsteady flow we introduce the following lower-deck variables

$$\bar{u}(x, y, t) = e^{-it} u(X, Y) + O(\epsilon), \quad (2.20)$$

$$\bar{v}(x, y, t) = \epsilon^2 e^{-it} v(X, Y) + O(\epsilon^3), \quad (2.21)$$

$$\bar{p}(x, y, t) = \epsilon e^{-it} p(X) + O(\epsilon^2). \quad (2.22)$$

In these expressions we have utilized the fact that since the unsteady flow is governed by the linearized Navier-Stokes equations we can seek solutions which have a harmonic time dependence.

Substituting (2.13), (2.20) - (2.22) into (2.6) - (2.8) yields, to leading order in ϵ ,

$$-i\epsilon^2 Su + Uu_X + uU_X + Vv_Y + vU_Y = -p_X + u_{YY}, \quad (2.23)$$

$$u_X + v_Y = 0 . \quad (2.24)$$

As noted in the Introduction, our interest in this paper is in the relatively high frequency case where we choose Ω to be of the same order as the Tollmien-Schlichting wave frequency at and upstream of the lower branch of the neutral stability curve. For this reason we require that $\Omega = O(\epsilon^2)$ i.e., the Strouhal number $S = O(\epsilon^{-2})$. Thus we define a scaled Strouhal number S_0 such that

$$S_0 = \epsilon^2 S, \quad S_0 = O(1). \quad (2.25)$$

Furthermore, in this case the Stokes-layer thickness is found to be of $O(\epsilon)$ also, and, therefore, it will be of $O(\epsilon^5)$ in terms of the lower-deck scalings. Hence the Stokes-layer thickness is the same as that of the lower deck. Upstream of the triple-deck region, where the mean flow changes on the scale of x , the unsteady flow in the boundary layer is given by the Stokes solution, which can be written in terms of the lower-deck scalings, as

$$u = 1 - e^{i^{3/2} S_0^{1/2} Y}, \quad (2.26)$$

$$p = i X S_0 . \quad (2.27)$$

The lower-deck problem is completed by solving (2.23), (2.24) using (2.25) subject to the no slip condition at the wall

$$u = v = 0 \quad \text{on } Y = F(X) , \quad (2.28)$$

matching with the main-deck solution

$$u \rightarrow 1 + a(X), \quad Y \rightarrow \infty, \quad \text{all } X, \quad (2.29)$$

and matching with the upstream Stokes layer solution given by (2.26) and (2.27) for $X \rightarrow -\infty$. Finally, the relationship between $a(X)$ and dp/dX is given by the interaction condition

$$d^2 a/dX^2 = 1/\pi \int_{-\infty}^{\infty} [dp/d\xi - i S_0] / (\xi - X) d\xi . \quad (2.30)$$

It was found that numerical solutions of the disturbance equations were not obtainable for supercritical disturbances using the interaction law (2.30). Thus an alternative method used by Bodonyi & Duck (1985) in treating three-dimensional interacting flows has been employed here. In this approach, the relationship between the pressure $p(X)$ and displacement thickness $-a(X)$ is found through a numerical solution of the upper-deck equations as opposed to the Hilbert integral representation (2.30). Specifically, it can be shown that the appropriate boundary-value problem in the upper-deck for the disturbance pressure is given by

$$\hat{p}_{XX} + \hat{p}_{\hat{y}\hat{y}} = 0 , \quad (2.31)$$

with boundary conditions

$$\hat{p}_{\hat{y}}(X, 0) = d^2a/dX^2 , \quad (2.32)$$

$$\hat{p}(X, \hat{y}) \rightarrow 0, \quad \hat{y} \rightarrow \infty, \quad \text{all } X , \quad (2.33)$$

$$\hat{p}(X, \hat{y}) + iS_0 X \rightarrow p(X) \quad \text{as } \hat{y} \rightarrow 0, \quad (2.34)$$

$$\hat{p} \rightarrow 0 \quad \text{as } X \rightarrow -\infty, \quad (2.35)$$

$$\hat{p}_X - ik\hat{p} \rightarrow 0, \quad \text{as } X \rightarrow \infty, \quad (2.36)$$

where we've written

$$p - p_\infty = \epsilon [\hat{p}(X, \hat{y}) + iS_0 X] , \quad \hat{y} = y/\epsilon^3 . \quad (2.37)$$

Note that (2.36) defines a radiation condition applied on the disturbance pressure at the downstream boundary to simulate the outward propagating pressure disturbances there. The wave number, k , which depends on S_0 , is found from the solution of the classical Orr-Sommerfeld eigenvalue problem for the Stokes' layer flow.

Alternatively, k can be computed iteratively from the numerical computations, as will be discussed below.

The entire unsteady solution is thus known once the solution of this boundary-value problem has been obtained. As a special case Goldstein (1985) gives an analytical solution to the problem using a linearized solution of the steady-flow problem for a slightly cranked flap on a flat plate due to Stewartson (1970,1971). Utilizing these results for $U(X,Y)$, $V(X,Y)$ and $P(X)$ Goldstein was able to solve the unsteady problem using a Fourier transform technique.

In this paper we solve the corresponding problem for surface distortions such that the steady flow is fully nonlinear in character. However, in this case both the steady and the unsteady problems must be solved numerically. Before discussing the numerical approach used in this study it is appropriate to note that the problem formulated above differs in a significant way from the usual hydrodynamic stability problem which generally involves the solution of the Orr-Sommerfeld equation. The Orr-Sommerfeld eigenvalue problem when applied to boundary-layer flows leads to the solution for "free" disturbances which are, in fact, the normal modes of the boundary layer and they are usually referred to as the Tollmien-Schlichting waves. While important in their own right, the normal mode representation of a small disturbance spectrum cannot be conveniently extended to finite-amplitude, i.e., nonlinear disturbances, nor are they useful by themselves in understanding how external disturbances, such as free-stream turbulence or surface

roughness, etc, feed energy into the boundary layer, thereby exciting spatially growing T-S waves.

One approach to understanding both the linear and nonlinear evolution of T-S waves in a boundary layer is to consider an initial-value problem, using the unsteady triple-deck equations. Such studies have been carried out recently by Smith (1985), Smith & Burggraf (1985), and Duck (1985).

Alternatively, one can study the nature of the coupling between an imposed free-stream disturbance and the growth of T-S waves in the boundary layer. This receptivity problem differs from the hydrodynamic stability problem both physically and mathematically. Physically, it is the response in the boundary layer to some externally imposed disturbance. Mathematically, it is no longer an eigenvalue problem. Instead it is a boundary-value problem as can be seen from equations (2.23) - (2.24) and (2.26) - (2.30), wherein the boundary layer is driven by some external forced oscillation with its response being a solution of the linearized disturbance equations having the same frequency and phase speed as the particular forcing disturbance being studied. The primary objective of this work is a detailed numerical study of this receptivity problem for a range of values of S_0 , which represents the nature of the freestream disturbance, and a representative surface distortion which we take to be

$$F(X) = h(1 + X^2)^{-1} , \quad (2.38)$$

where h is an order one factor which gives the height of the distortion relative to the lower-deck scalings.

3. Numerical Method

3.1 Steady-State Solution

First we consider the steady flow problem defined by equations (2.14) - (2.19) along with (2.38). Numerical solutions have been found using a finite-difference procedure developed by Smith & Bodonyi (1985). Briefly, the governing equations are replaced by difference representations for ψ , $U = \psi_Y$, $\tau = U_Y$, and P with uniform steps in X , Y . The computational domain extends from $X = X_1$ (<0) to $X = X_2$ (>0) and from $Y = 0$ to $Y = Y_\infty$, with starting conditions (2.17) specified, in effect, at $X = X_1$.

The nonlinear difference equations at a given streamwise location X are solved to within a tolerance of 10^{-6} in absolute value by Newtonian iteration using Gaussian elimination and back substitution. The solution is then advanced to the next streamwise location and the process repeated until the entire domain is covered. Since the problem is interactive, multiple forward-marching sweeps are necessary until a tolerance of 10^{-5} between successive values obtained for $P(X)$ is satisfied for all X . At this point the solution is said to have converged in the global sense. The diagonally dominant nature of the finite-difference form of the interaction law (2.19) makes this multi-sweeping process both fast and stable. Whenever flow reversal occurs, i.e., $U < 0$, windward differencing is used to represent UU_x in finite-difference form.

The numerical solution has been found using (2.38) for the surface shape with $h = 0.1, 1.0$ and 5.0 . Representative

distributions of the wall shear $\tau(X,0)$, and pressure, $P(X)$, of the steady flow are given in Figure 2 for $h = 5.0$.

With the steady solution known, we now proceed to consider the numerical solution of the complex unsteady linearized boundary-layer equations (2.23) - (2.24). In our approach, the governing equations were solved in the physical plane using a finite difference method.

3.2 Unsteady Solution

The unsteady equations (2.23) - (2.24) were replaced, after subtracting out the Stokes shear-wave solution, by a system of difference equations of second-order accuracy to be consistent with the numerical method used for the steady flow problem. Since the governing equations are linear no iteration in the normal direction is necessary at a fixed streamwise location. A single sweep across the boundary-layer region was sufficient to determine the solution there. Thus one complete sweep of the computational domain could be accomplished quickly. Multiple sweeps of the entire domain are still necessary to obtain the global solution, however, due to the elliptic nature of the interaction law (2.30) or equations (2.31) - (2.36).

Initial attempts to solve the problem were made using the pressure-displacement interaction law (2.30) in a form utilizing the ideas first put forward by Veldman (1979) and fully discussed by Smith & Bodonyi (1985). Indeed, for values of $S_o \leq 1$ acceptable solutions could be found. However, as the scaled frequency, S_o , was increased towards its critical (i.e. neutral) value of $S_{o\text{crit}} \approx 2.296$ acceptable numerical solutions became increasingly more difficult to obtain. It appears that these difficulties are related to the use of

the interaction condition (2.30). Numerically, the Hilbert integral is truncated to the finite range $X_1 \leq \xi \leq X_2$, thus it is implicitly assumed that the tails of the integral over $-\infty < \xi < X_1$ and $\xi > X_2$ are negligibly small. This assumption appears to be satisfactory for the upstream "tail", but it is questionable for the downstream behavior of the integral. Furthermore, in addition to the difficulties associated with the finite integration domain, there is some question as to the convergence properties of the Cauchy-Hilbert integral itself, at least when the disturbances are supercritical, due to the exponentially growing form of the disturbance quantities downstream.

To overcome these difficulties, the method developed by Bodonyi & Duck (1988) for solving flows with viscous-inviscid interaction has been successfully applied to this problem. In this method the relationship between the disturbance pressure and displacement thickness is found through a numerical solution of the appropriate upper-deck equations (2.31) - (2.36) as opposed to the Hilbert integral representation of the solution, equation (2.30). The crucial feature of the scheme is the inherent numerical coupling between the viscous boundary-layer solution and the inviscid outer flow solution which is carried out simultaneously in the spirit of the scheme proposed by Veldman (1979). Using this approach, the difficulties associated with the convergence of the Hilbert integral for supercritical disturbances can be avoided and the proper downstream boundary condition (radiation condition, see 2.36) can be applied to the disturbance pressure.

For numerical convenience we apply the Prandtl transposition law and we also subtract out the Stokes solution. Thus consider the following change of variables

$$u(X,Y) = 1 - e^{i^{3/2}S_0^{1/2}Y} + u_0(X,Y) , \quad (3.1)$$

$$v(X,Y) = v_0(X,Y) , \quad dp/dX - iS_0 = dp_0/dX , \quad (3.2)$$

Then the disturbance equations can be written as

$$u_{0X} + v_{0Y} = 0 , \quad (3.3)$$

$$(U_X - iS_0)u_0 + Uu_{0X} + U_Yv_0 + Vu_{0Y} + dp_0/dX - u_{0YY} = -U_X + [U_X + i^{3/2}S_0^{1/2}V]e^{i^{3/2}S_0^{1/2}Y} , \quad (3.4)$$

with boundary conditions

$$u_0 = v_0 = 0 \quad \text{on } Y = 0, \text{ all } X , \quad (3.5)$$

$$u_0 \rightarrow 0 \quad \text{as } X \rightarrow -\infty , \text{ all } Y , \quad (3.6)$$

$$u_0 \sim a(X) + e^{i^{3/2}S_0^{1/2}Y} \quad \text{as } Y \rightarrow \infty , \text{ all } X. \quad (3.7)$$

Given a guess or an update for u_0 , v_0 , $p_0(X)$ and $\hat{p}(X, \hat{Y})$ everywhere, equations (3.3) - (3.7) are marched forward in X , while simultaneously equations (2.31) - (2.36) are solved along a line of varying \hat{Y} . This then determines the complex-valued functions u_0 , v_0 , p and \hat{p} (and hence $a(X)$) at a given streamwise location X . Sweeping through all X stations constitutes one global iteration. Convergence is finally attained when a global convergence test on the disturbance displacement thickness $-a(X)$ is satisfied.

The main features of the numerical scheme are the following. Two and three-point differencing in Y is used for equations (3.3) and (3.4), respectively, with equation (3.7) applied at $Y = Y_0$. Three-point central differencing is used to approximate (2.31) in both dimensions, while condition (2.33) is applied at $\hat{Y} = \hat{Y}_0$. Equation

(2.32) is approximated by one-sided differencing in \hat{y} and a second-order scheme for X derivatives. Finally, the radiation condition is applied in the following form to estimate the disturbance pressure at the downstream boundary

$$\hat{p}(X_{\max}, \hat{y}) = [\hat{p}(X_{\max} - 2\Delta X, \hat{y}) - 4\hat{p}(X_{\max} - \Delta X, \hat{y})] / [2ik\Delta X - 3] .$$

The value for k is either prescribed as discussed earlier, or by estimating its value from the relation $(\partial \hat{p} / \partial X) / i\hat{p}$ from values of X reasonably far downstream, and then feeding this value back into the numerical computations. Numerically, the results indicate only slight differences in estimating k in these two ways. This isn't too surprising since the viscous-inviscid interaction is a local phenomenon and the behavior far downstream should approach that of the classical stability theory.

Supposing we have n points in Y and m points in \hat{y} , then at each X station, the difference approximation of equations (3.3), (3.4) and (2.31), together with the interface conditions (2.34) and (3.7) can be written conveniently in matrix form as discussed by Bodonyi & Duck (1988). The overall scheme is nominally second-order accurate in the grid spacings ΔX , ΔY and $\Delta \hat{y}$. The resulting matrix equation is then solved using standard Gaussian elimination procedures and back substitution.

4. Numerical Results

In this section the results of the numerical computations will be presented. As part of a collaborative effort to confirm the finite-difference numerical solutions, Dr. P.W. Duck and Mr. J.W.C. Welch of the University of Manchester, Manchester, England, have solved the same receptivity problem discussed in the previous section using both time-marching and time-periodic spectral methods. These spectral computations were not supported by this NASA grant. However, in the figures that follow, the finite-difference results are represented by solid curves and the spectral results by the symbol o for comparison purposes. A detailed discussion concerning the spectral method as applied to this problem can be found in Bodonyi, Welch, Duck and Tadjfar (1989).

We first consider the effect of the Strouhal number, S_o , on the interaction between the unsteady flow and the surface distortion. To minimize any nonlinear effects, a small value of the hump height, $h = 0.1$, for which separation does not occur in the mean flow, was chosen. The numerical solution was found for several values of S_o , ranging from 0.5 to 3.5. In most cases 200 points were taken in the streamwise direction over the range $-10 \leq X \leq 10$ ($\Delta X = 0.10$). To solve the lower-deck equations, 50 points were taken across the lower-deck region over the range $0 \leq Y \leq 7.5$. Also, an additional 50 points were used in the upper-deck \hat{y} scaling over the range $0 \leq \hat{y} \leq 5$, to solve Laplace's equation for the pressure in the upper-deck region. To test the sensitivity of the thickness of the upper-deck region, in

some cases the upper-deck range was extended to $\hat{y} = 10$ (100 points), but no significant differences in the results were noticed.

Using the finite difference method of solution, convergence of the numerical computations was achieved when the absolute value of the difference in the displacement thickness, $-a(X)$, between two successive iterates was less than 10^{-5} for all X . The number of iterations required for convergence was found to be quite sensitive on the value of S_0 under consideration and also on the initial guesses taken for the disturbance profiles. For a subcritical disturbance of $S_0 = 0.5$, less than one hundred iterations were sufficient for convergence. However, for a supercritical disturbance with $S_0 = 3.0$ approximately 3400 iterations were necessary to obtain converged results. Also, by gradually increasing the value of S_0 and using the converged solution for the previous value of S_0 as the initial guess, we could reduce the number of iterations required and also maintain a small maximum fluctuation between successive iterative values of the displacement thickness.

The disturbance produced by the interaction with the hump should ultimately decay sufficiently far downstream of the hump if the scaled freestream Strouhal number is below its critical value, $S_{0crit} = 2.296$. To illustrate this eventual damping of the unsteady disturbances, an extended range of $-10 \leq X \leq 40$ ($\Delta X = 0.25$) was considered. The real parts of the complex-valued disturbance pressure and wall shear distributions for a representative subcritical case, $S_0 = 2$, are presented in Figure 3 from both the finite difference and spectral methods. The decay in the disturbance

amplitude for all quantities is clearly seen for $X \geq 10$. Similarly, the disturbances should amplify downstream of the surface distortion if S_0 is supercritical. The same extended X range was thus considered for a typical supercritical case, $S_0 = 2.5$ and Figure 4 shows the amplification of the disturbances in the streamwise direction in this case.

The supercritical results given in Figure 4 were calculated using a linearized time-marching scheme and are shown for $t = 14\pi$. For both cases, excellent agreement exists between the finite difference and spectral method results for the positioning of the T-S waves. There is a discrepancy of approximately 10% in the wave amplitudes. This difference can be reduced by increasing the number of grid points in the X direction of the finite difference method as discussed below.

Numerical experiments using the finite difference method indicate that we can enhance the convergence rate in subcritical cases by extending the X -domain. The further downstream we place the boundary, the more the disturbance is damped near the boundary and this, in turn, speeds up the global convergence properties of the scheme. Conversely, for supercritical disturbances the further away the downstream boundary is placed, the larger the value of the disturbance amplitude becomes, and this results in a further increase in the number of iterations required for convergence.

We next consider the nonlinear problem with a hump height of $h = 1.0$. In this case the mean flow is still attached everywhere in the flowfield. The disturbance solution for this case has the same shape

and follows the same pattern as the previous solutions for $h = 0.1$ over the entire range of Strouhal numbers considered in this study. However, now the amplitudes of the disturbances are increased by a factor of approximately 10, which indicates a linear mechanism for the amplification of the disturbances due to increasing the height, at least for this range of values of h .

The growth rate, k_i , and the wavelength, λ , of the T-S waves can be calculated from the numerical results and compared with the values given by the analytical theory (Duck 1985). The pressure $\bar{p}(X,t) = \text{Real}(\bar{p}_1(X)e^{-it})$, where $\bar{p}_1(X)$ is calculated numerically. Now $\bar{p}_1(X) = Ce^{ikX} +$ a function of X which decays algebraically as $X \rightarrow \infty$ and C is a constant. Therefore, $(d\bar{p}_1/dX)/\bar{p}_1 \approx ik$ and $(d^2\bar{p}_1/dX^2)/\bar{p}_1 \approx -k^2$, where $k = k_r + ik_i$ and $\lambda = 2\pi/k_r$. This approximate method for calculating k should become more accurate when k is calculated from higher order derivatives of the pressure. Figures 5a,5b show the values obtained at each X station for the linearized time-periodic spectral results for the case $S_0 = 1.0$ calculated from the second derivative of the pressure. For comparison purposes, the finite difference results for k calculated using the first derivative approximation for the pressure are also shown. The two methods give substantially the same results for $X > 10$. In the region $12 < X < 40$ the values of k_r are within 3% of the analytical value of $k_r \approx -0.522$ and the values of k_i within about 10% of $k_i \approx 0.121$. The reason for the larger % error in k_i compared to k_r is that $|k_i| < |k_r|$. As is to be expected, as we move upstream of this region the algebraic terms become significant as the influence of the hump

increases and the calculated values of k_r , k_i show greater variation from their analytical values.

Figure 6 shows the results obtained for $h = 1.0$, $S_o = 3$. The finite difference results were calculated using an X grid $-10 \leq X \leq 15$ with $\Delta X = 0.125$. The time-marching spectral method results here are for $t = 5\pi$ (with the negative of the results plotted for comparison with the finite difference solution). By this time the time-periodic solution is established in the region approximately $X < 13$ and here there is excellent agreement with the finite difference results.

Next, results for $h = 5$, for which the mean flow has a small region of separated flow, are presented. In Figure 2, the corresponding mean flow distributions for the pressure and wall shear are presented. We note that the solutions obtained by the finite difference method and the steady spectral method are in excellent agreement. There are some small oscillations in the wall shear results in the reversed flow region suggesting the need for a somewhat finer grid for the finite difference method. This effect was confirmed by running the finite-difference code on a somewhat finer grid ($-10 \leq X \leq 10$, 400 points). In this case the oscillations noted above did indeed disappear.

For this value of h , the finite difference method was used to obtain converged solutions for $S_o = 1$ and 1.2. Pressure and wall shear distributions for the unsteady flow over the X-domain, $-10 \leq X \leq 10$ is given in Figure 7 for $S_o = 1$.

Converged solutions using the finite difference method for larger values of the Strouhal number are possible in principle; however, the computer time necessary to achieve them becomes prohibitive. Furthermore, the accuracy of the numerical solutions deteriorates as the streamwise step size, ΔX , is increased. This deterioration can best be seen in the wall shear results. Maintaining the same number of mesh points (200) and increasing ΔX we have been able to find three other "numerically converged" solutions for $h = 5$ and $S_o = 1$. The wall shear distributions for these solutions are given in Figure 8. Note that for all cases the general shape of the solutions do not change. However, by increasing ΔX the magnitude of the disturbance amplitude was reduced while maintaining its same form and location. For the largest value of ΔX , which corresponds to an X domain of $-10 \leq X \leq 90$ ($\Delta X = 0.50$), the numerical breakdown is clearly seen in Figure 8c even though the general shape of the distribution has not changed appreciably. For this same X-domain, another "numerical solution" was obtained for half the step size by doubling the number of points to 400 and the results are shown in Figure 8d. Note that the numerical oscillations have disappeared and the same general shape of the curve remains. However, the magnitude of the amplitude is the same as that in Figure 8b. There thus seems to be a trade-off between a larger X-domain to help on the convergence rate and a smaller step size to maintain an accurate solution.

For $h = 5$, $S_o = 1$, the finite difference results calculated on the three grids: $-10 \leq X \leq 40$, $\Delta X = 0.25$; $-10 \leq X \leq 20$, $\Delta X = 0.15$;

and $-10 \leq X \leq 10$, $\Delta X = 0.1$; giving discrepancies in the amplitude of the T-S wave of up to 30%, 10% and 5%, respectively, when compared with the time-periodic spectral method results which were calculated on a grid sufficiently fine and extensive to give grid independent results to graphical accuracy. A comparison of these results for the spectral method and the finite difference method using the third grid is also given in Figure 7.

A comparison between the numerical computations and Goldstein's (1985) analytical theory for $h \ll 1$ can also be made. The disturbance amplitude computed is shown in Figures 9a,b for $h = 1$, $S_0 = 3$ and $h = 5$, $S_0 = 1.2$, respectively. For $h = 1$, the analytical theory and the numerical results are in good agreement over most of the region of interest. For smaller values of h and other values of S_0 , not shown here, indicate an even better agreement between the two approaches. Thus we can conclude that the analytical theory can be applied for $h < 1$. Conversely, for $h = 5$, the disturbance amplitude predicted by Goldstein's theory does not agree well with that predicted by the numerical computations. The nonlinear base flow results in substantial differences of the receptivity problem from that computed by the analytical theory.

We next consider the physical implications of the numerical results, and in particular the effect of the hump height, h , on the disturbance wave amplitude. We choose to follow the amplitude variation with h of several peaks in the disturbance wall shear solution. These peak values are scaled by the corresponding peak values of the linear results: Note that the location of the peaks

does vary slightly with h . The peak amplitude dependence on h was studied for subcritical values of S_0 , namely $S_0 = 1, 2$ and for the supercritical value $S_0 = 3$. The $S_0 = 3$ solutions were found for $h \leq 3.5$, calculations for larger values of h were affected by a grid dependent rapid growth in the spectral plane solution for $|k| \gg 1$. This possible Rayleigh instability (see Smith & Bodonyi 1985, Tutty & Cowley 1986) is suppressed in the time-periodic spectral method and the finite-difference method which treats the "steady-state" equations to find solutions which are periodic in time. Consequently, solutions can be found for $1 \leq h \leq 5$.

In Figures 10a,b we show the results for $S_0 = 1$ and $S_0 = 3$, giving the scaled peak amplitude behavior for the wall shear $\bar{\tau}(x, 0)$ with h for two different peaks; the results for $S_0 = 2$, not presented here, follow a similar pattern.

For $h < 1$, the scaled disturbance amplitude depends approximately linearly on the hump height. Experimentally, Azin & Polyakov (1979) found a linear dependence of the disturbance amplitude on h , for the interaction of upstream propagating sound waves with thin mylar strips fixed on a flat plate near the lower branch of the neutral stability curve. For larger values of h , our results show an increasingly nonlinear enhancing effect on the disturbance amplitude. These results are confirmed by the finite difference results for $S_0 = 1$. For example, for $h = 3$ the disturbance amplitude is approximately twice that of the linear results for the same h . The results for the subcritical S_0 calculated using the time-periodic spectral method and finite difference method show that this increasingly rapid

enhancement of the "receptivity" continues for $h = 4$ and 5 . The results for $h = 4, 5$ are approximately three and six times, respectively, the corresponding linear results for the same h .

In conclusion we find a linear dependence of the disturbance amplitude on the hump height for sufficiently small values of h . For moderate h ($1 \leq h \leq 3$) we find an enhancement of the receptivity by the nonlinear effect of hump height. For large h where local flow separation can occur in the steady flow, we find a possible short wavelength instability in our time marching calculations and a rapidly increasing enhanced receptivity in our "steady state" calculations.

Acknowledgement

The author is grateful to the Ohio Supercomputer Center for making computer time available on the Cray X-MP computer during this research program.

REFERENCES

- Aizin, L.B. & Polyakov, N.F. 1979, (in Russian) Preprint 17, Akad. Nauk USSR, Siberian Div., Inst. Theor. Appl. Mech., Novosibirsk. (See also Nishioka, M. & Morkovin, M.V. 1986, *J. Fluid Mech.*, V. 171, 219).
- Bodonyi, R.J., Smith, F.T. & Gajjar, J. 1983, *IMA J. Appl. Math.*, V. 30, 1.
- Bodonyi, R.J. & Duck, P.W. 1988, *Computers & Fluids*, V. 16, 279.
- Bodonyi, R.J., Welch, J.W.C., Duck, P.W. & Tadjfar, M. 1989, *J. Fluid Mech.*, to appear.
- Burggraf, O.R. & Duck, P.W. 1981, Symp. on Physical Numer. Aspects Aerodyn. Flows, Calif. State Univ., Long Beach, Calif.
- Cooley, J.W. & Tukey, J.W. 1965, *Math. Comp.*, V. 19, 297.
- Duck, P.W. 1984, *Q. J. Mech. Appl. Math.*, V. 37, 57.
- Duck, P.W. 1985, *J. Fluid Mech.*, V. 160, 465.
- Duck, P.W. 1988, *J. Fluid Mech.*, V. 197, 254.
- Duck, P.W. 1989, *Computers & Fluids*, to appear.
- Duck, P.W. & Burggraf, O.R., 1986, *J. Fluid Mech.*, V. 162, 1.
- Gedney, C.J. 1983, *Phys. Fluids*, V. 26, 1158.
- Goldstein, M.E. 1983, *J. Fluid Mech.*, V. 127, 59.
- Goldstein, M.E. 1984, *J. Fluid Mech.*, V. 145, 71.
- Goldstein, M.E. 1985, *J. Fluid Mech.*, V. 154, 509.
- Goldstein, M.E., Sockol, P.M. & Sanz, J. 1983, *J. Fluid Mech.*, V. 129, 443.
- Goldstein, M.E., Leib, S.J. & Cowley, S.J. 1987, *J. Fluid Mech.*, V. 181, 485.
- Goldstein, M.E. & Hultgren, L.S. 1987, *J. Fluid Mech.*, V. 181, 519.
- Leehey, P. & Shapiro, P. 1979, In *Laminar-Turbulent Transition* (ed. Eppler, R. & Fasel), Springer, 321.
- Morkovin, M.V. 1969, Air Force Flight Dyn. Lab, Wright-Paterson AFB, Ohio, Rep. AFFDL-TR-68-149.

- Murdock, J.W. 1980, Proc. Roy. Soc. Lond., A372, 517.
- Reshotko, E. 1976, In Ann. Rev. Fluid Mech., V. 8, 311.
- Smith, F.T. 1973, J. Fluid Mech., V. 57, 803.
- Smith, F.T. 1985, United Technologies Research Center, Rept. UTRC85-36.
- Smith, F.T. & Bodonyi, R.J. 1982, J. Fluid Mech., V. 118, 165.
- Smith, F.T. & Bodonyi, R.J. 1985, Aeronautical J., V. 89, 205.
- Smith, F.T. & Bodonyi, R.J. 1987, Studies Appl. Math., V. 77, 129.
- Smith, F.T., Brighton, P.W.M., Jackson, P.S. & Hunt, J.C.R. 1981, J. Fluid Mech., V. 113, 123.
- Smith, F.T. & Burggraf, O.R. 1985, Proc. Roy. Soc. Lond., A399, 25.
- Stewartson, K. 1969, Mathematika, V. 16, 106.
- Stewartson, K. 1970, Q. J. Mech. Appl. Math., V. 23, 137.
- Stewartson, K. 1971, Q. J. Mech. Appl. Math., V. 24, 387.
- Tutty, O.R. & Cowley, S.J. 1986, J. Fluid Mech., V. 168, 431.
- Veldman, A.E.P. 1979, Netherlands Nat. Aerosp. Lab., NLR-TR-79023.

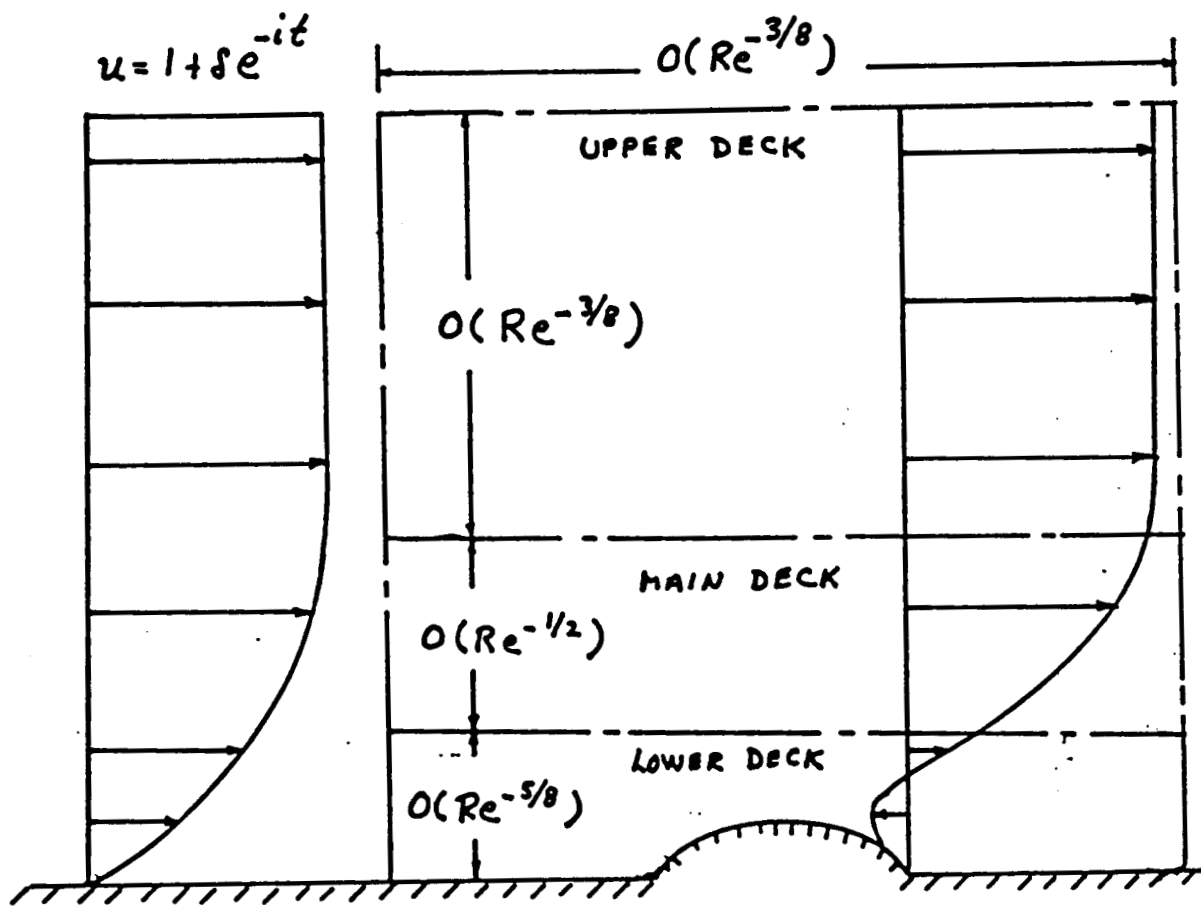


Figure 1. Schematic of the triple-deck flow structure.

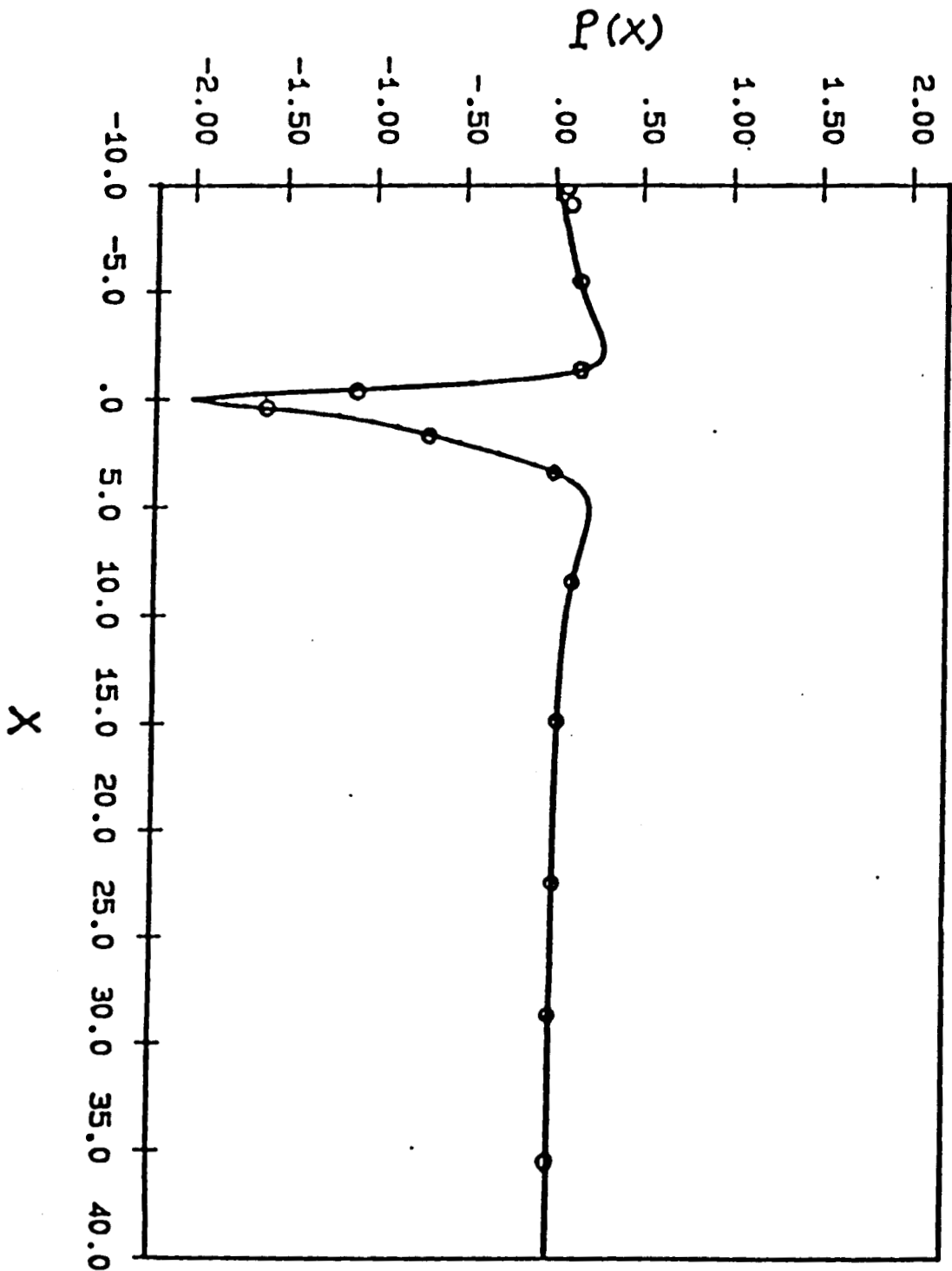


Figure 2a. Pressure distribution for steady flow with $h = 5$.
 — : finite-difference method; o : spectral method.

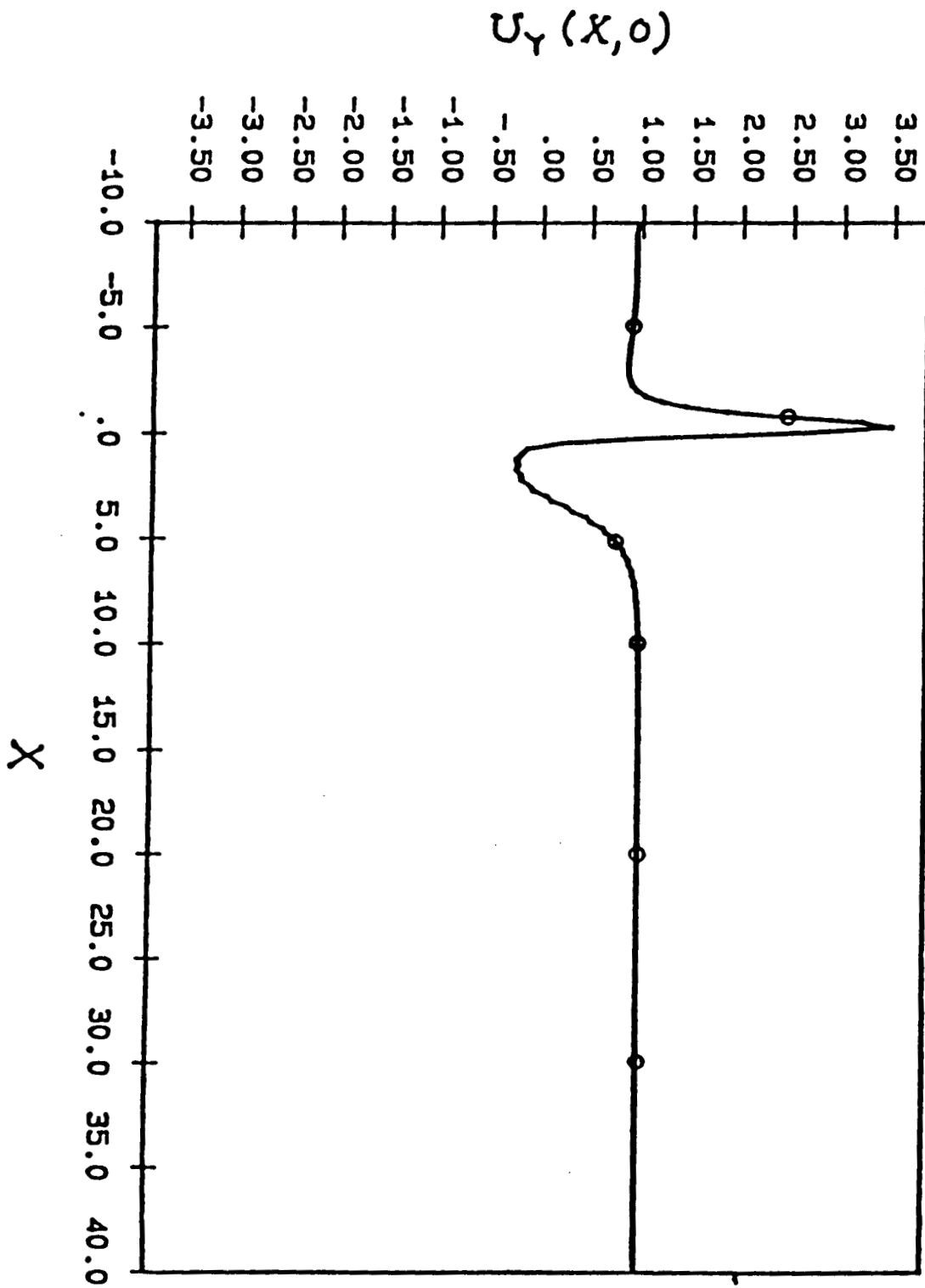


Figure 2b.

Wall shear distribution for steady flow with $h = 5$.
 — : finite-difference method; o : spectral method.

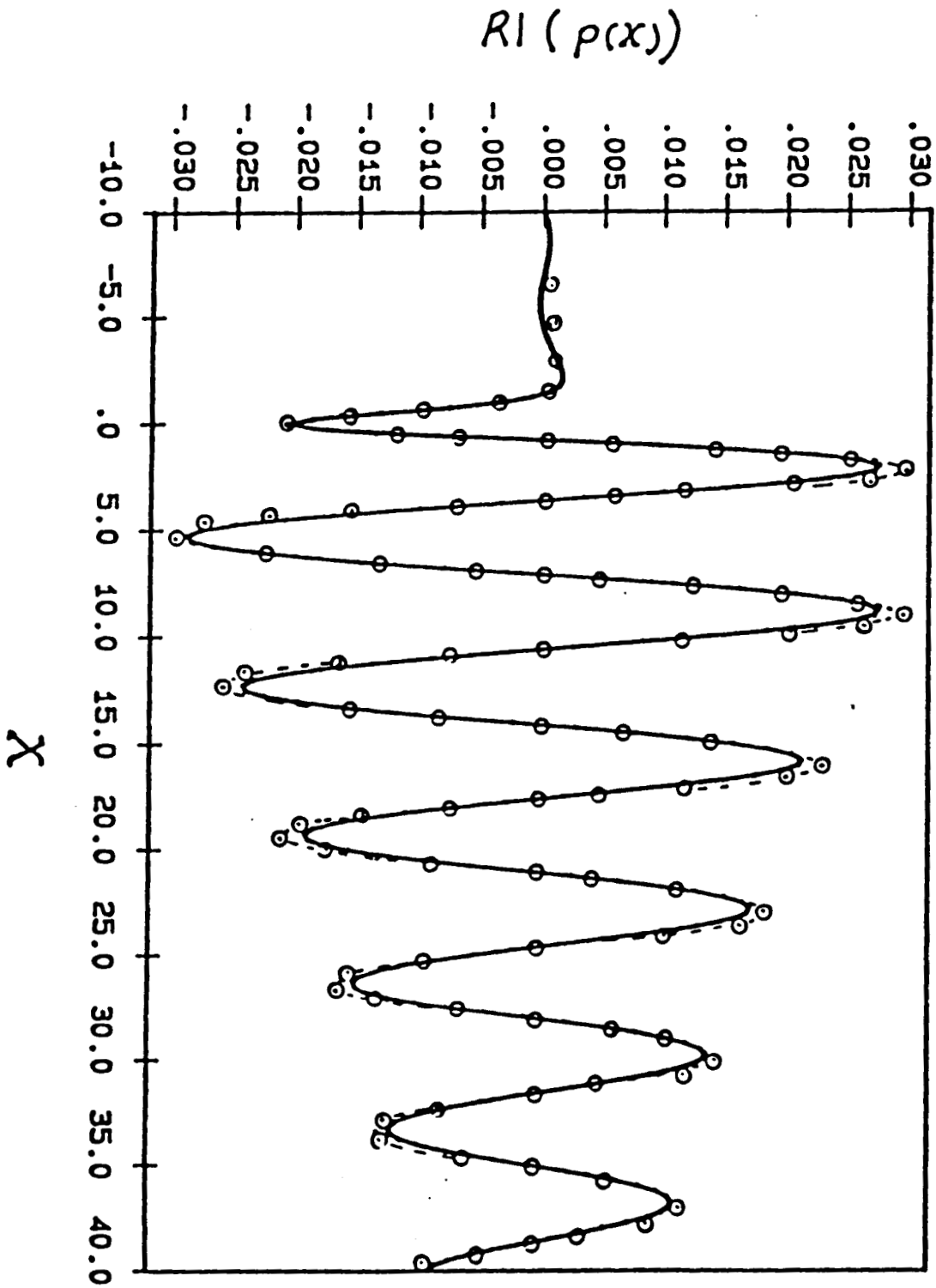


Figure 3a. Disturbance pressure for $S_0 = 2$, $h = 0.1$. — : finite-difference method; \circ : spectral method.

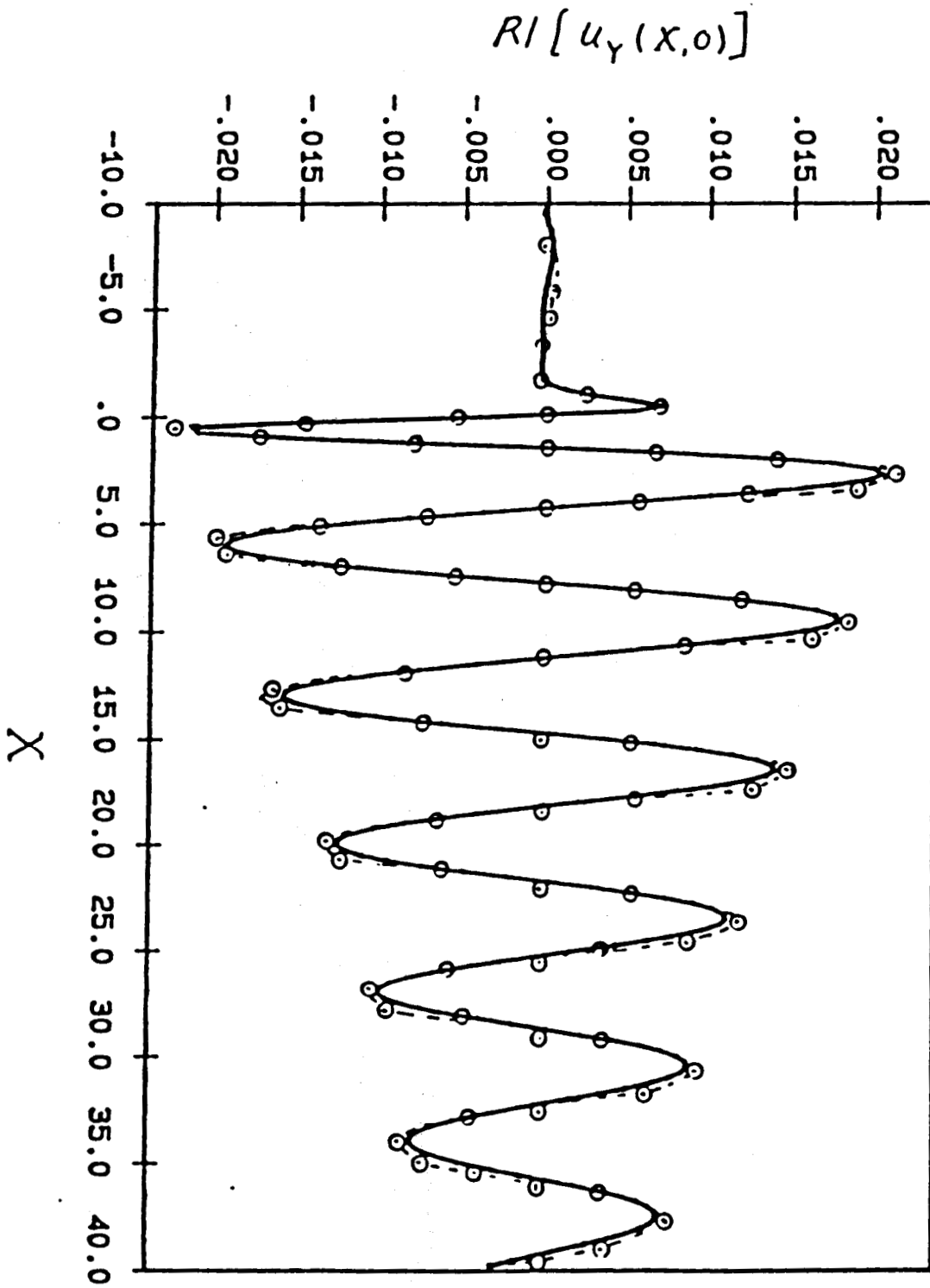


Figure 3b.

Disturbance wall shear for $S_0 = 2$, $h = 0.10$.

— : finite-difference method; o : spectral method.

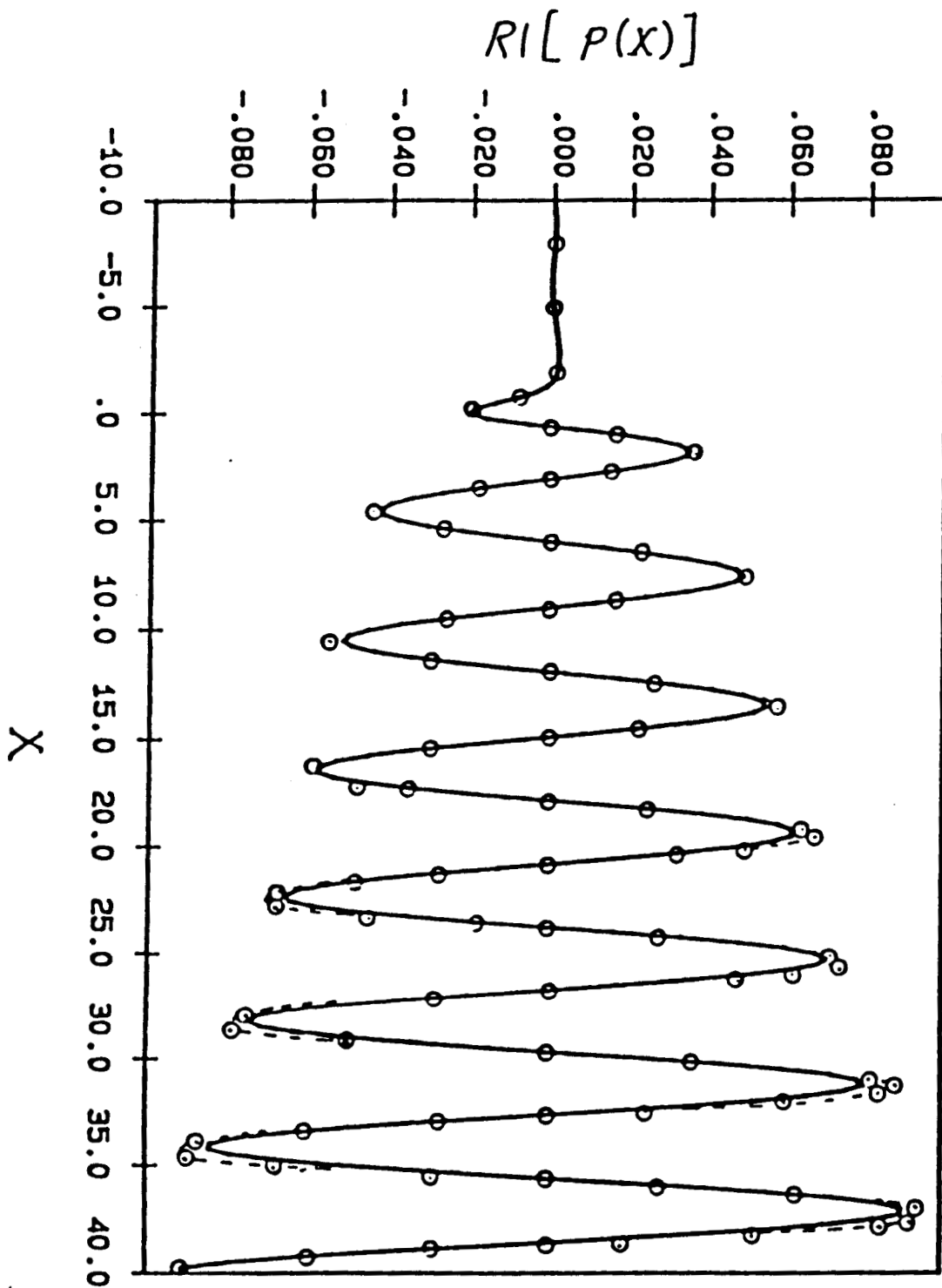


Figure 4a. Disturbance pressure for $S_v = 2.5$, $h = 0.10$.
 — : finite-difference method; o : spectral method.

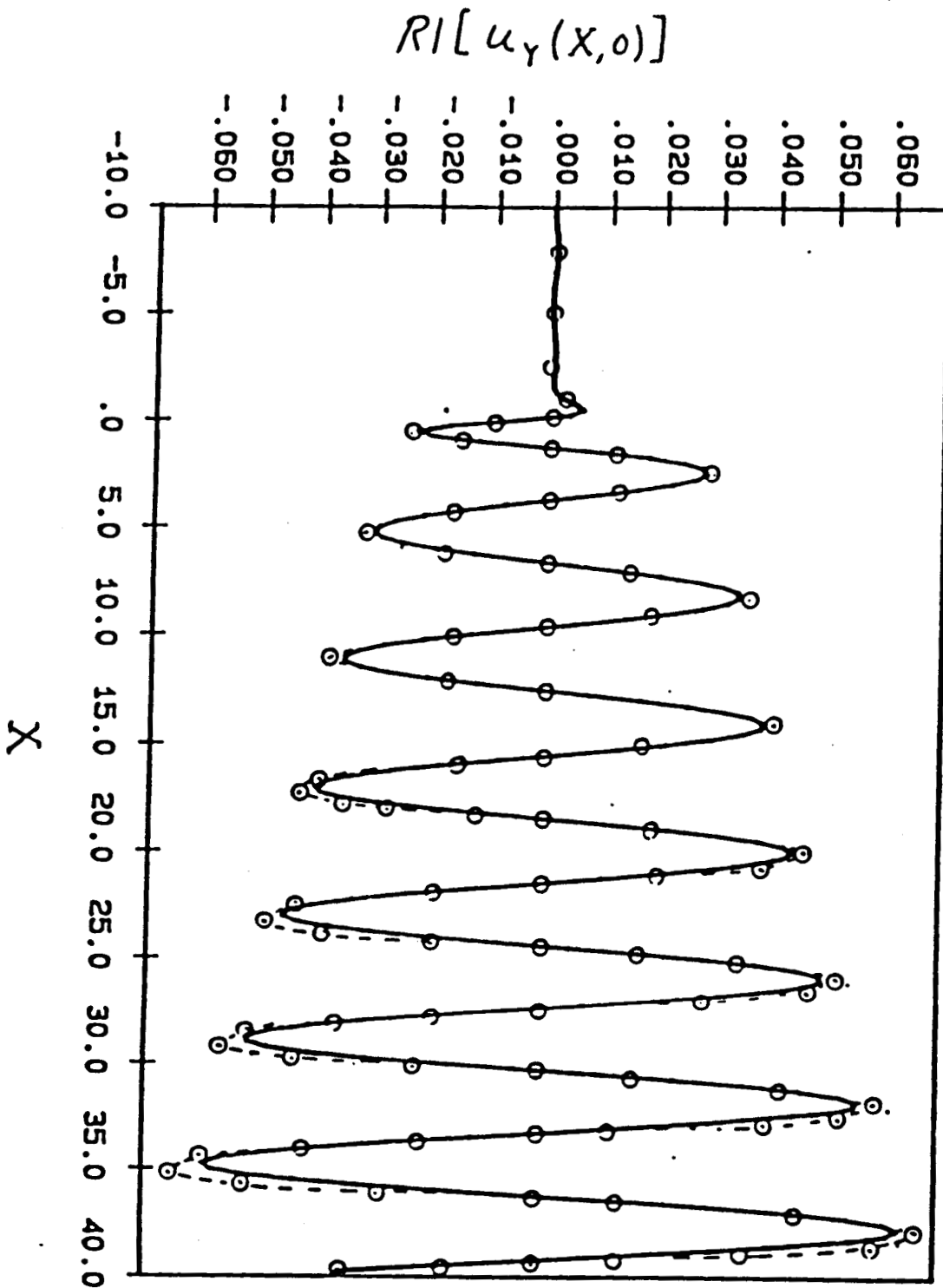


Figure 4b.

Disturbance wall shear for $S_\nu = 2.5$, $h = 0.10$.

— : finite-difference method; o : spectral method.

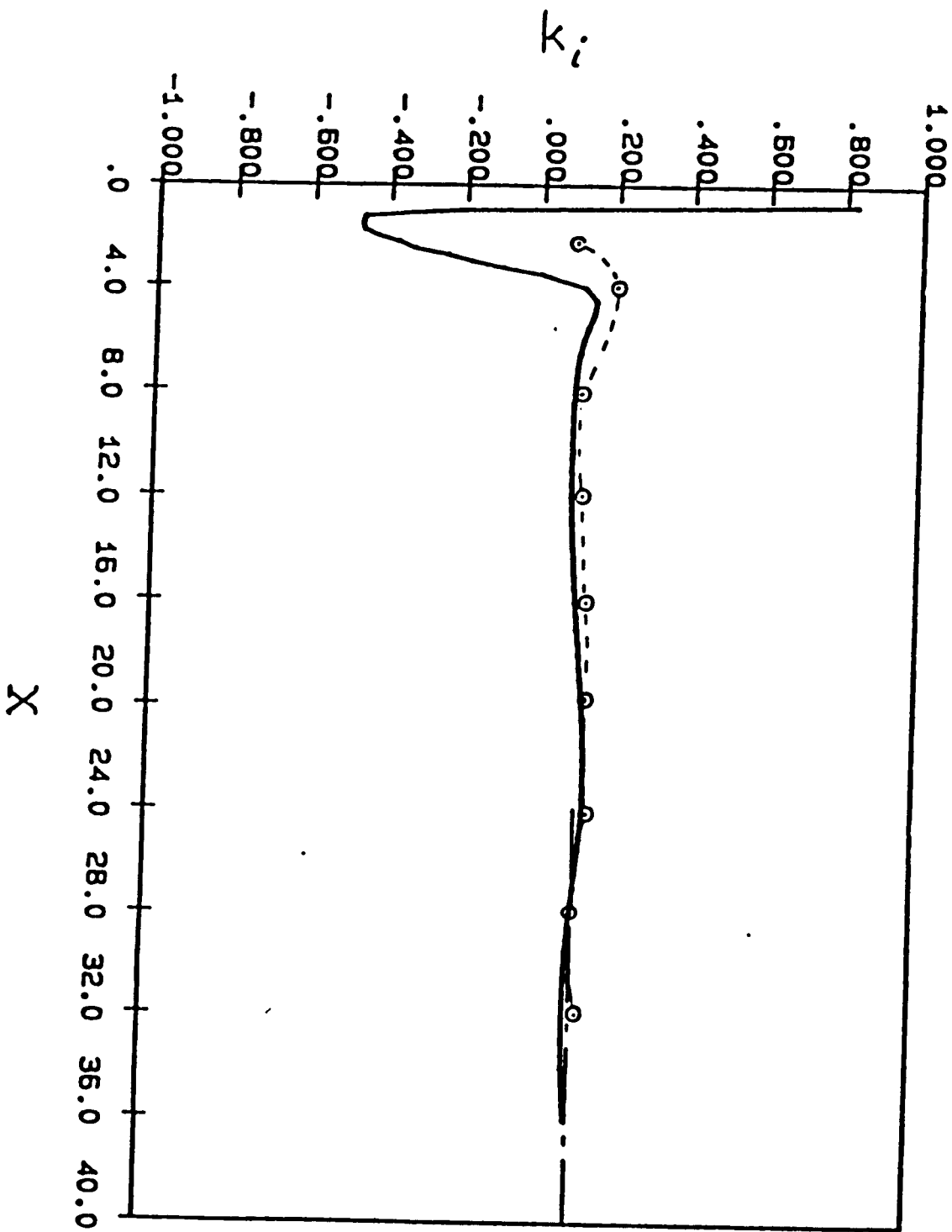


Figure 5a.

Tollmien-Schlichting wave growth rate.
 — : finite-difference method; o : spectral method;
 - - - : analytical value.

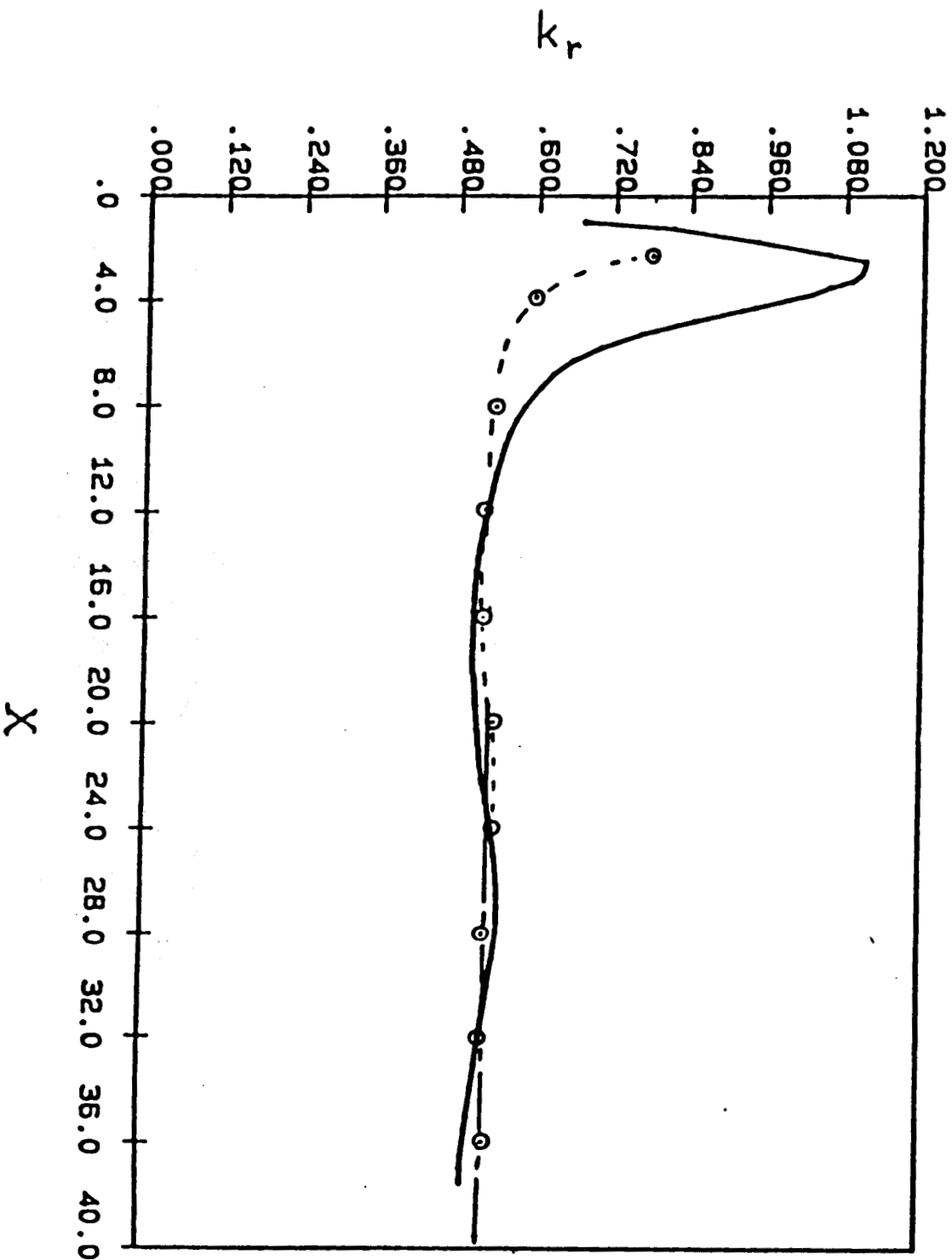


Figure 5b. Tollmien-Schlichting wavelength
 — : finite-difference method; o : spectral method;
 - - - : analytical value.

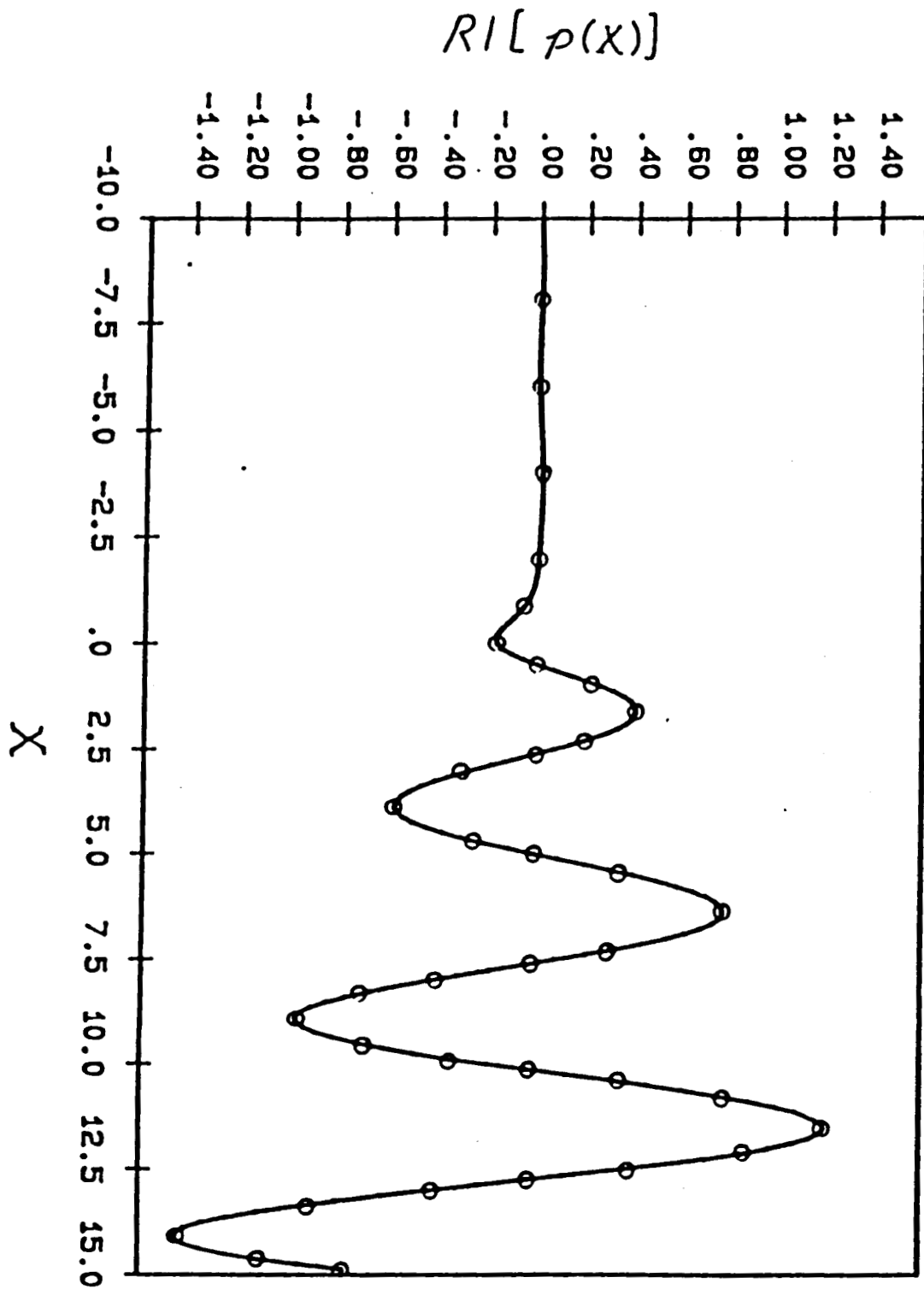


Figure 6a. Disturbance pressure for $S_0 = 3$, $h = 1$.
 — : finite-difference method; o : spectral method.

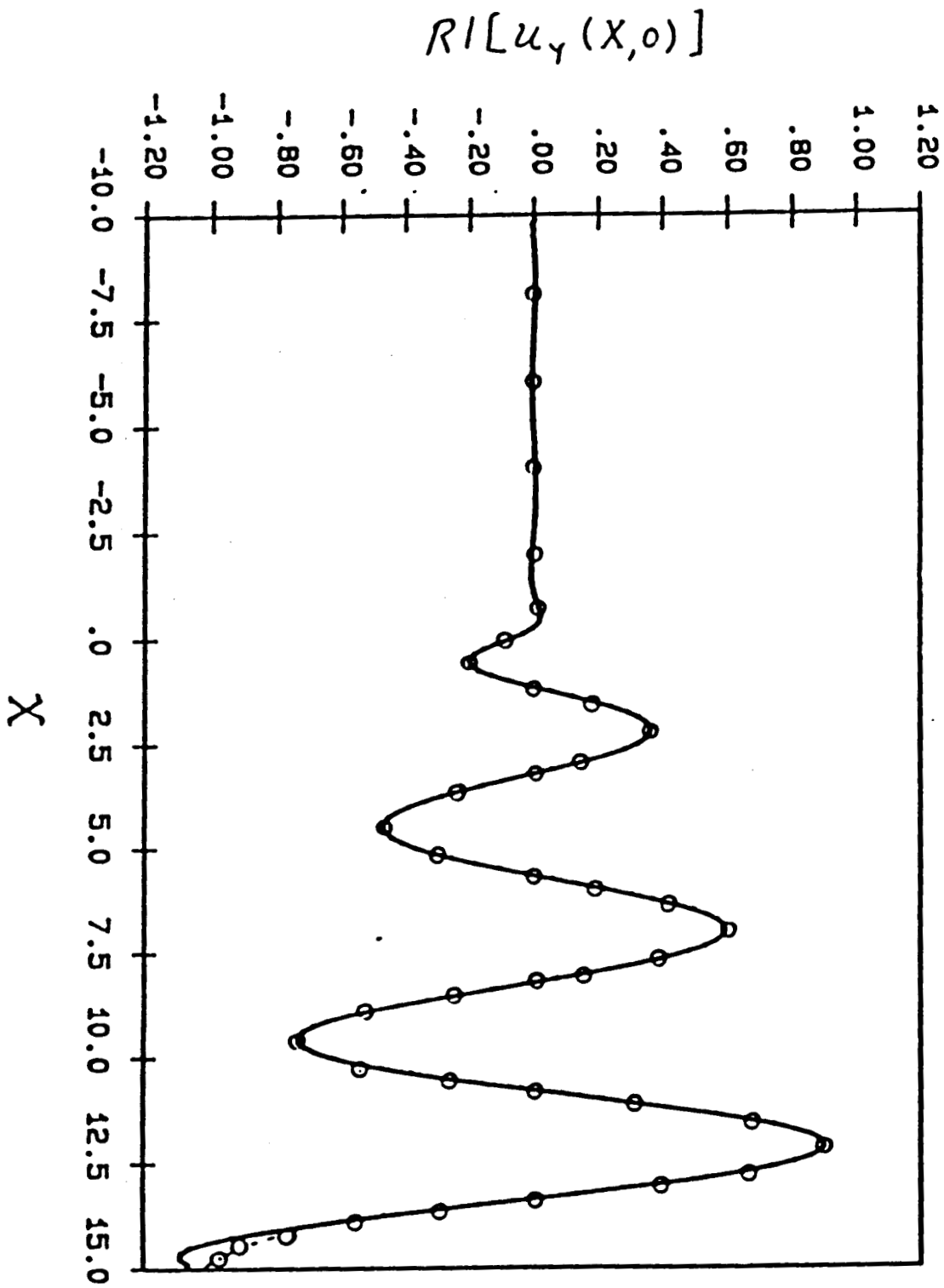


Figure 6b.

Disturbance wall shear for $S_0 = 3$, $h = 1$.

— : finite-difference method; o : spectral method.

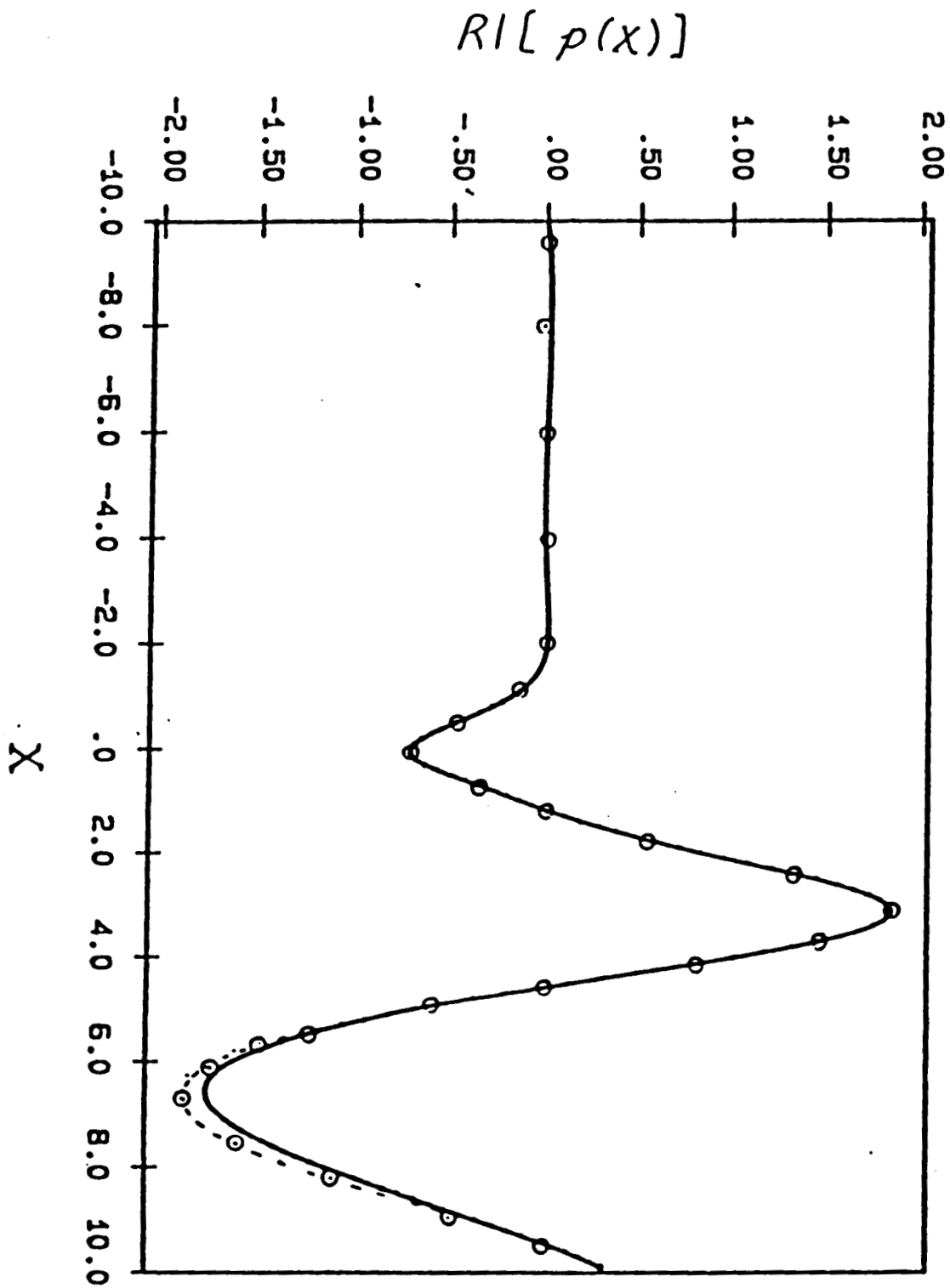


Figure 7a.

Disturbance pressure for $S_0 = 1$, $h = 5$.

— : finite-difference method; o : spectral method.

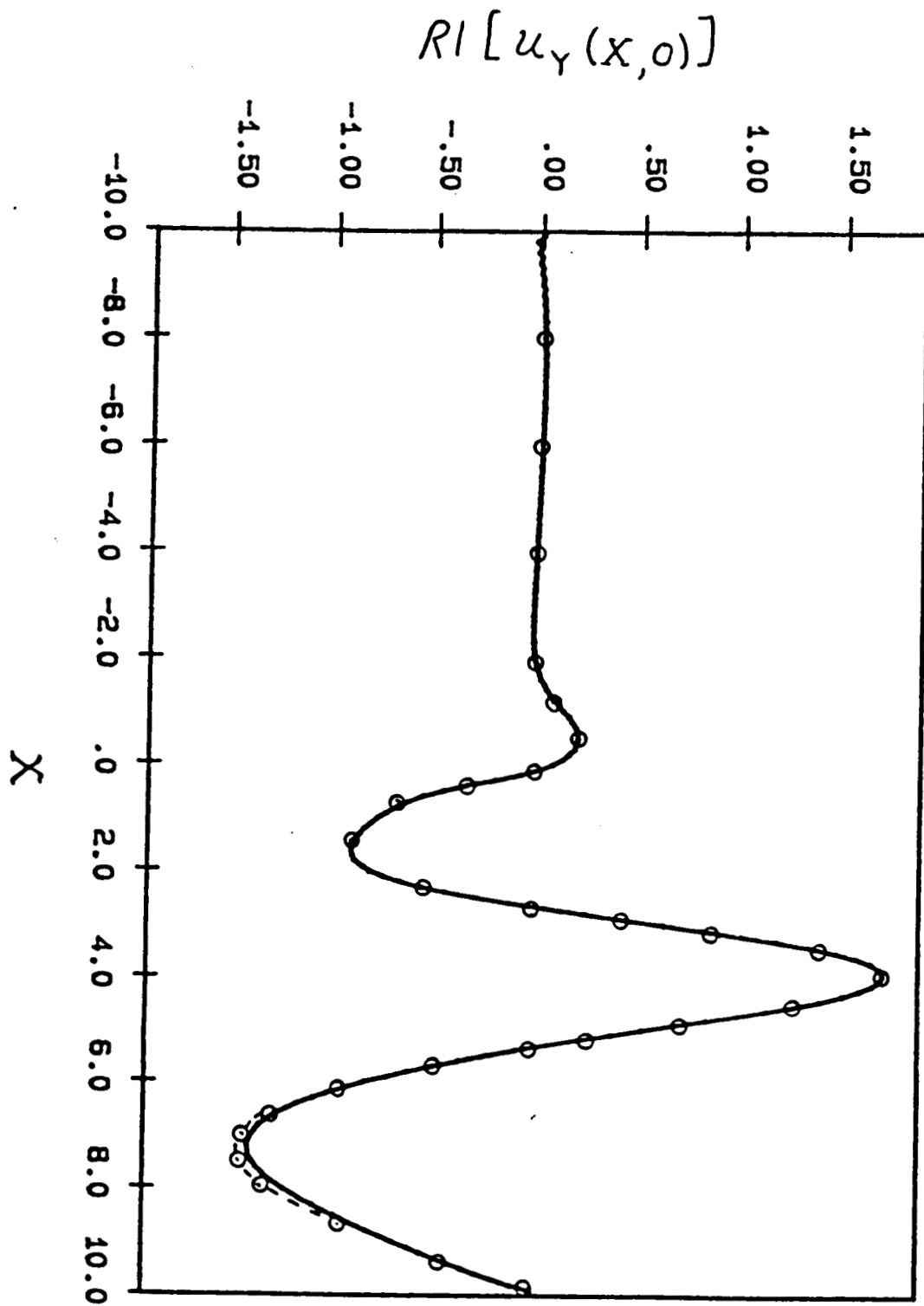


Figure 7b.

Disturbance wall shear for $S_0 = 1$, $h = 5$.

— : finite-difference method; o : spectral method.

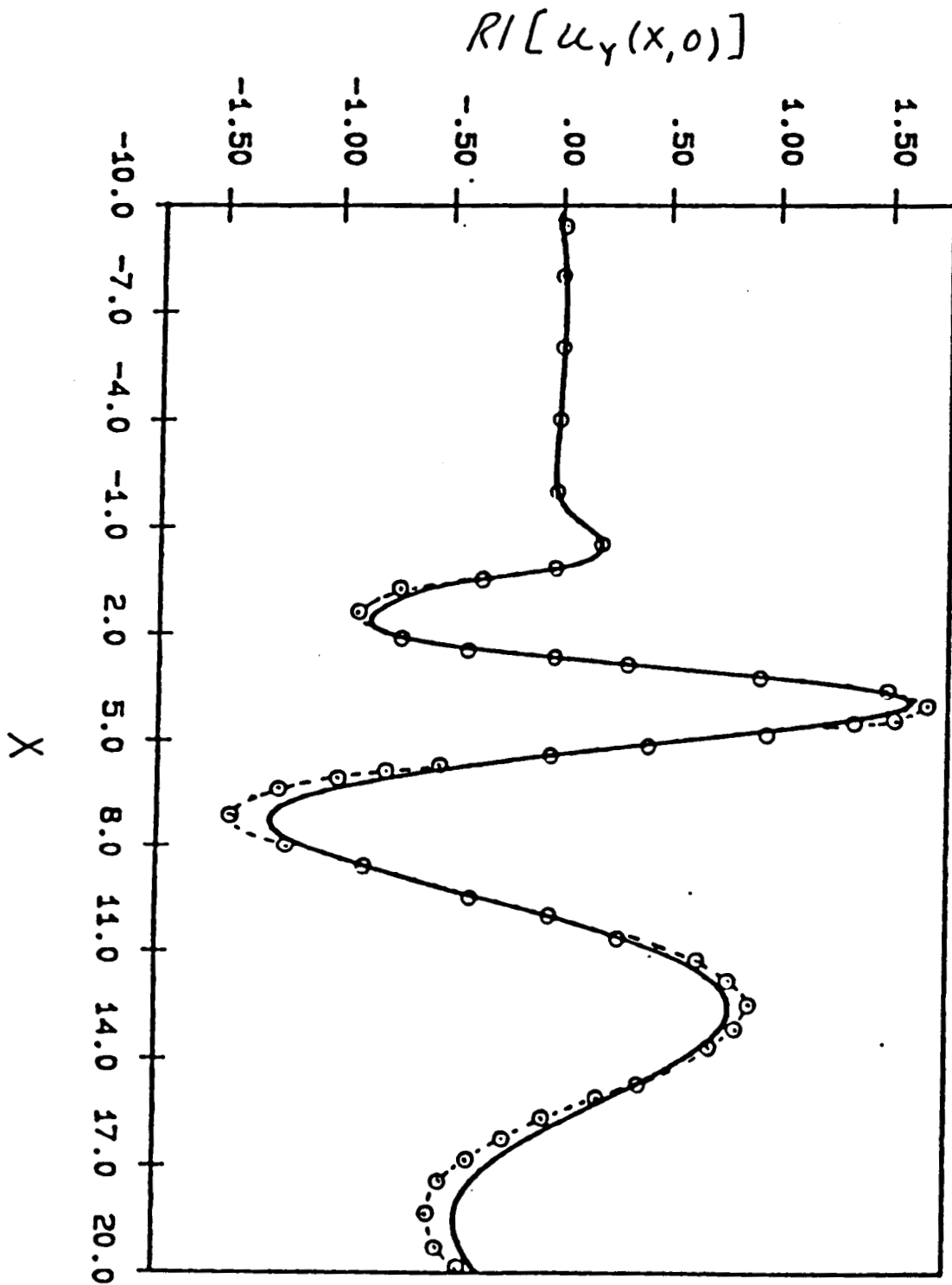


Figure 8a. Disturbance wall shear for $S_0 = 1$, $h = 5$ and X varying between $-10 \leq X \leq 20$.
 — : finite-difference method; o : spectral method.

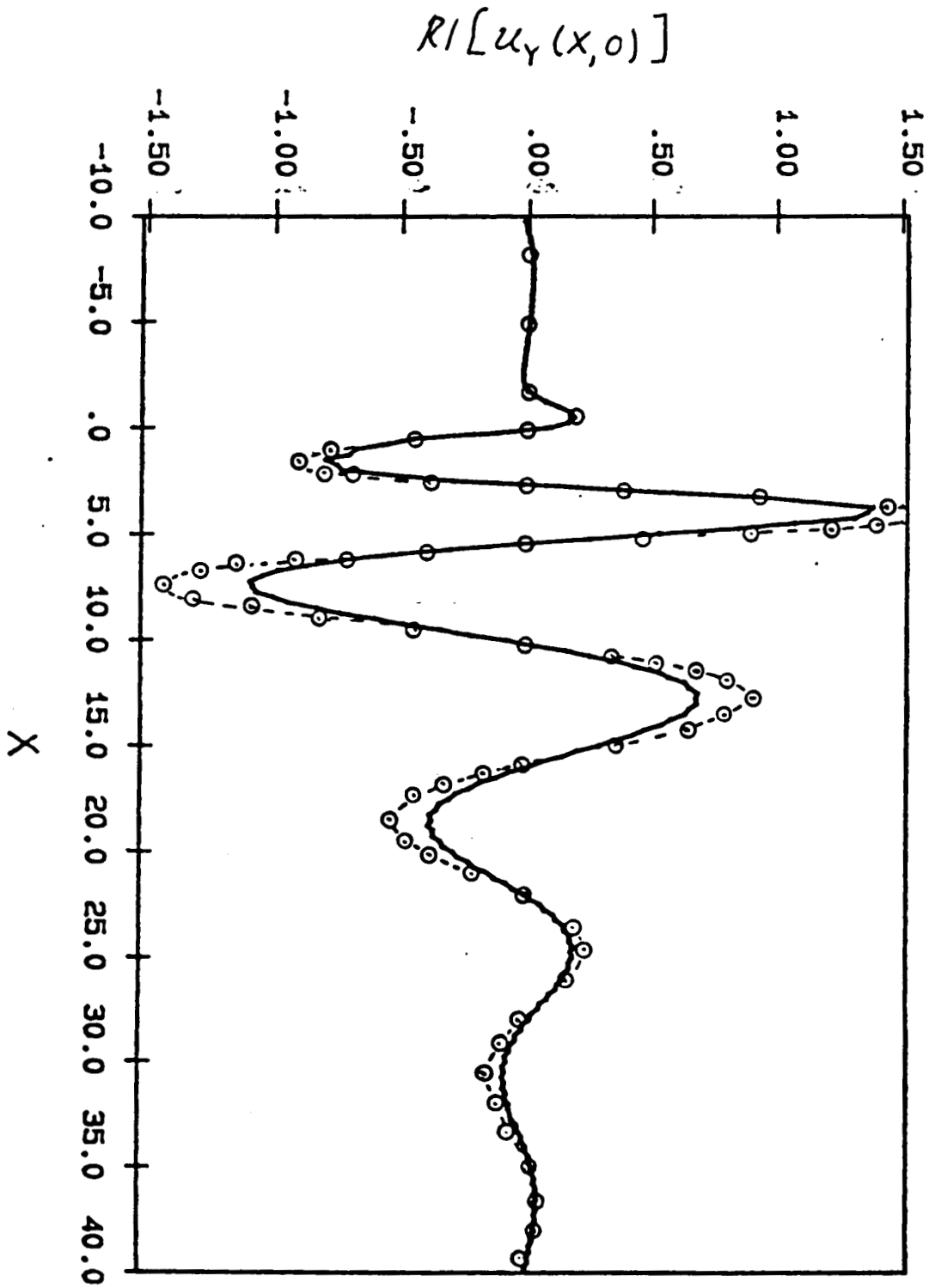


Figure 8b.

Disturbance wall shear for $S_0 = 1$, $h = 5$ and X varying between $-10 \leq X \leq 40$.

— : finite-difference method; o : spectral method.

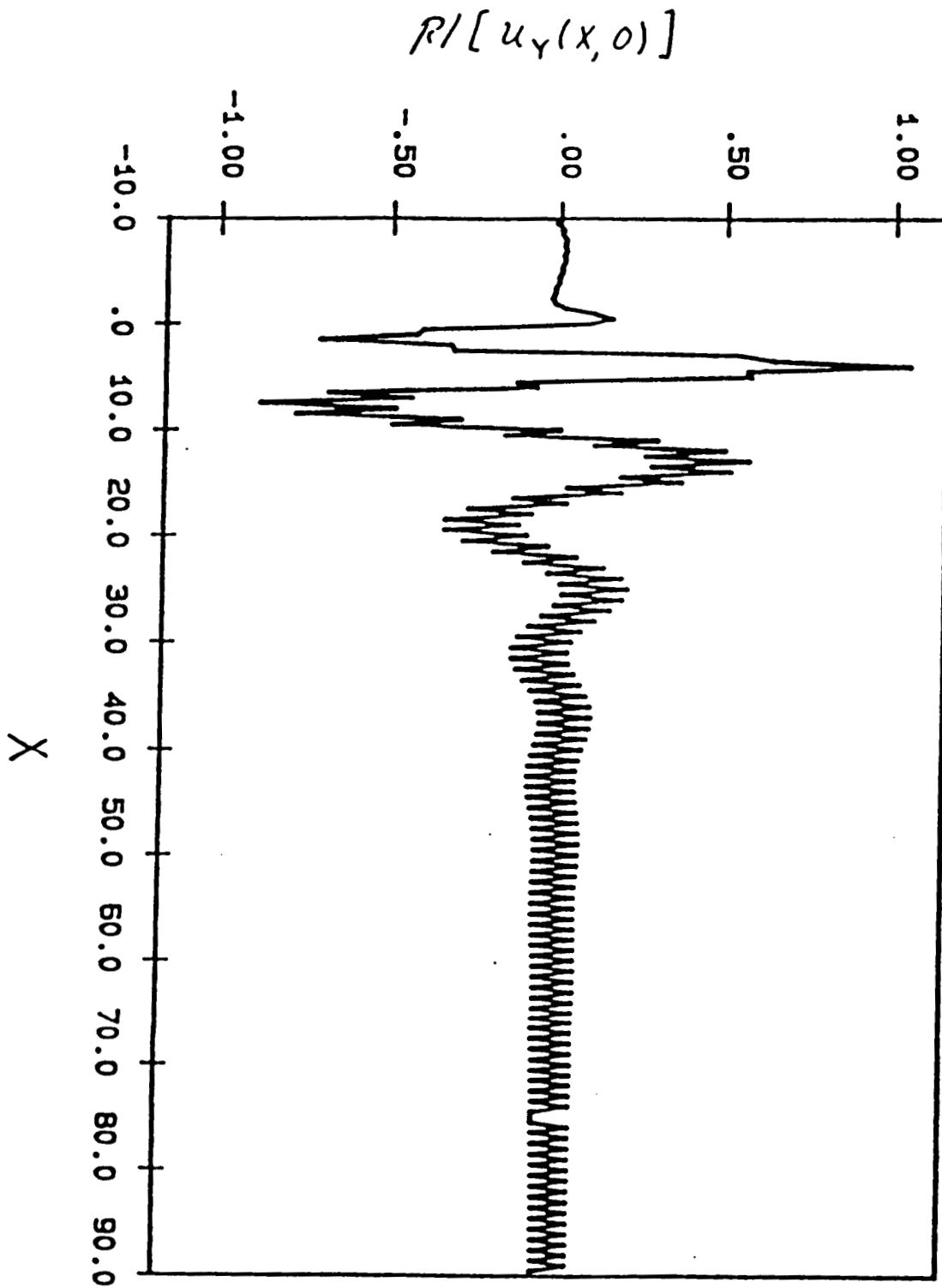


Figure 8c. Disturbance wall shear for $S_0 = 1$, $h = 5$ and X varying between $-10 \leq X \leq 90^\circ$ with $\Delta X = 0.50$.

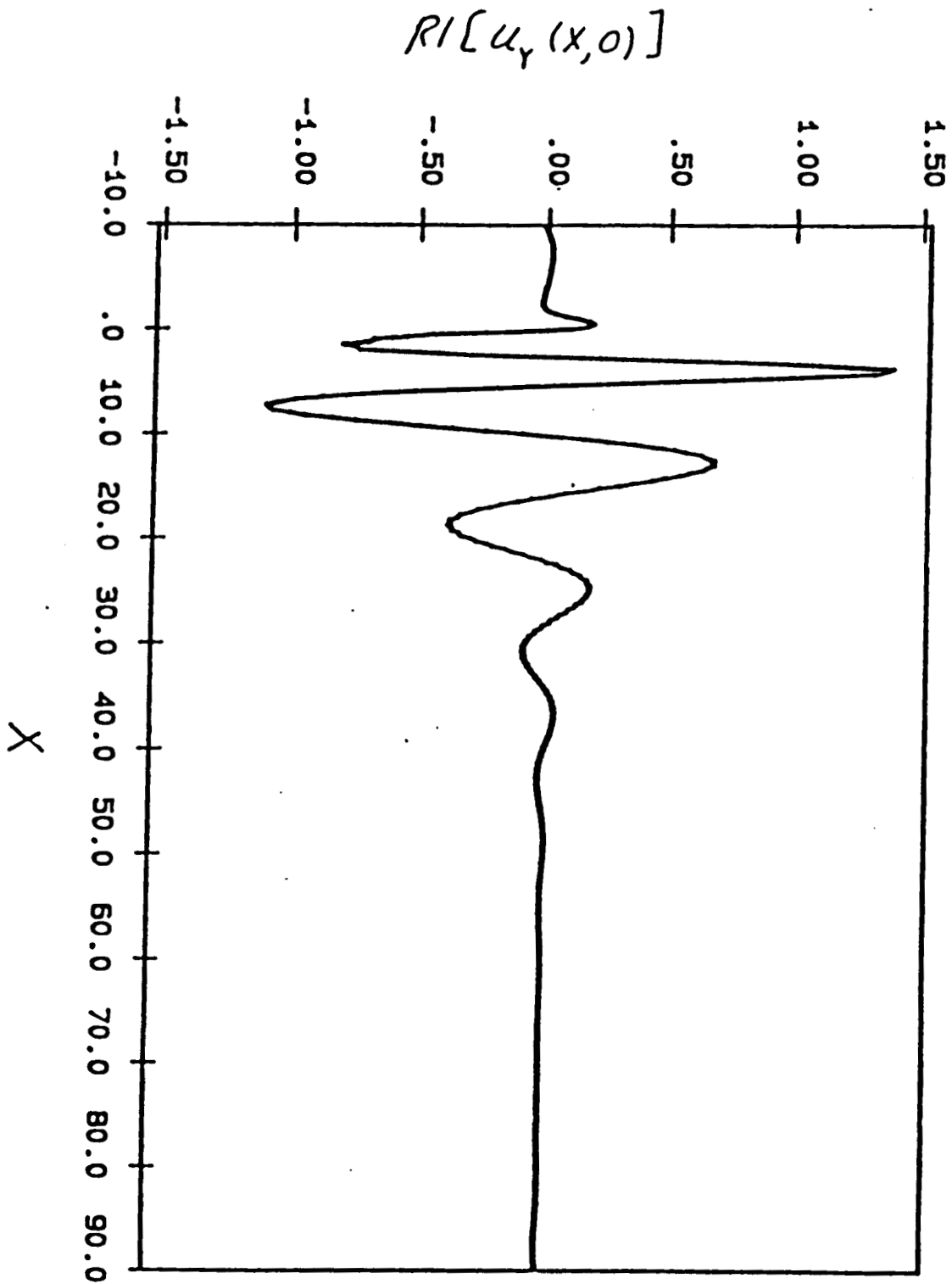


Figure 8d.

Disturbance wall shear for $S_0 = 1$, $h = 5$ and X varying between $-10 \leq X \leq 90^\circ$ with $\Delta X = 0.25$.

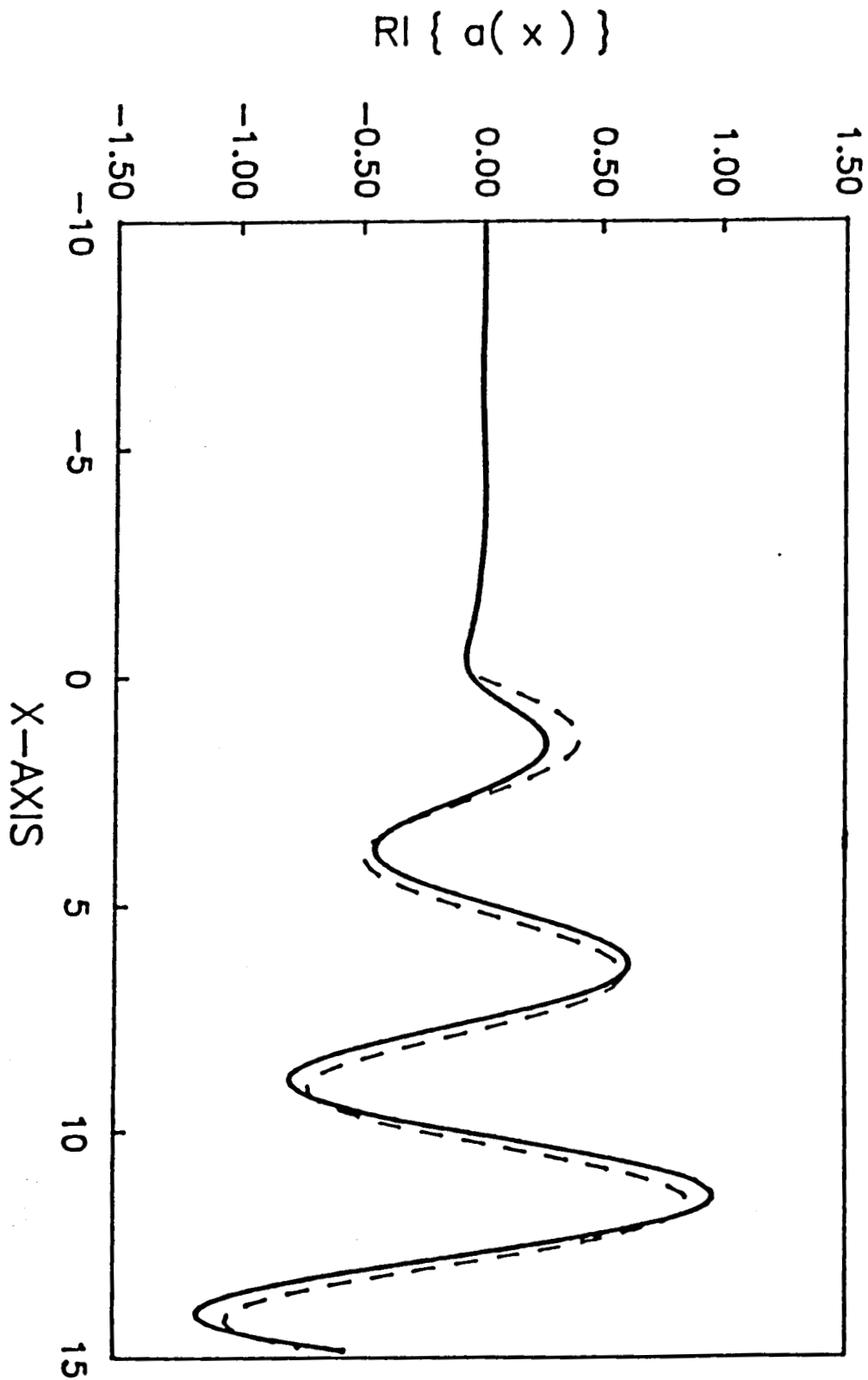


Figure 9a.

Comparison of disturbance displacement distribution for $h = 1$, $S_0 = 3$ computed by the finite difference method (—) and the analytical theory (- - -).

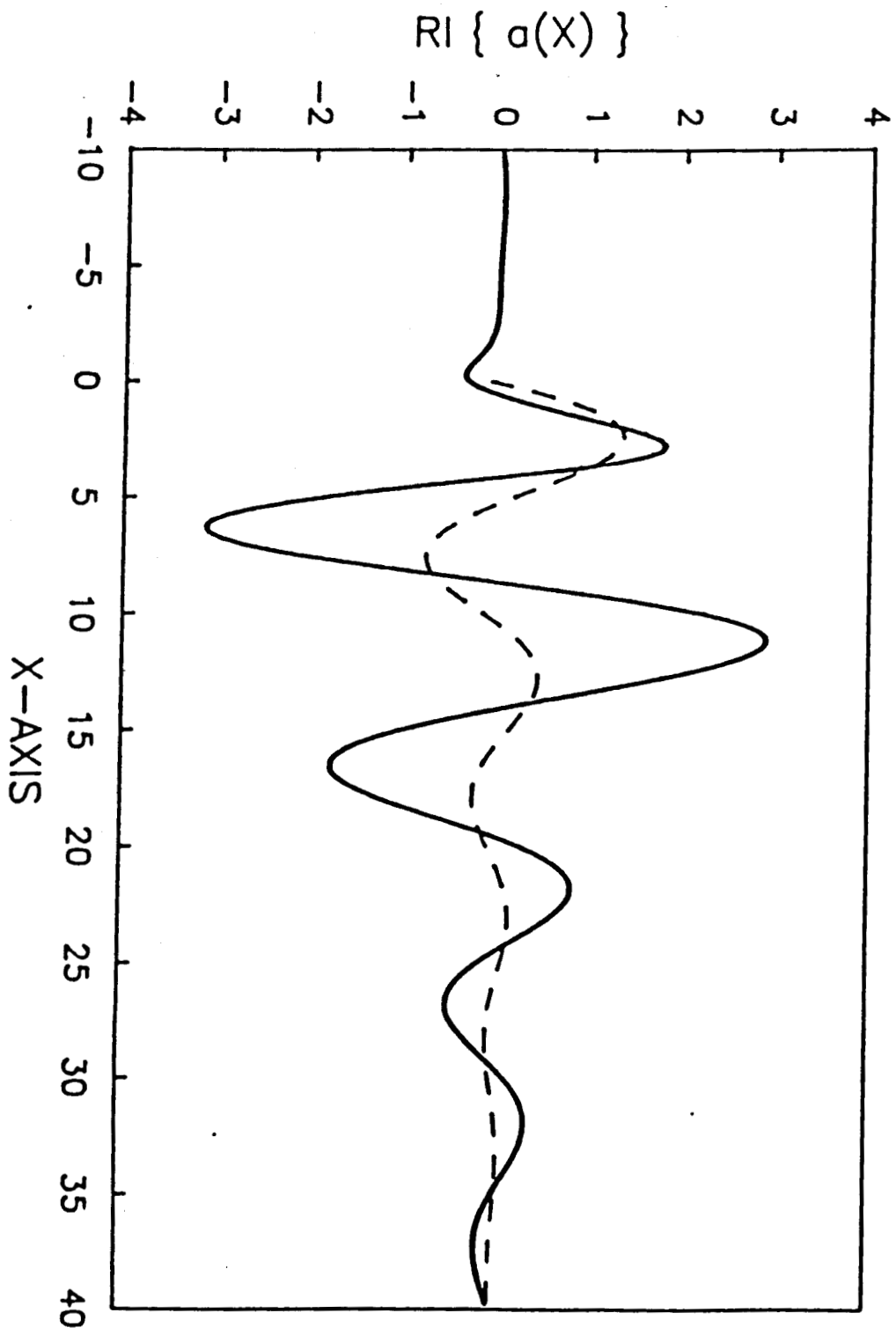


Figure 9b.

Comparison of disturbance displacement distribution for $h = 5$, $S_0 = 1.2$. : finite difference method; - - - : analytical theory.

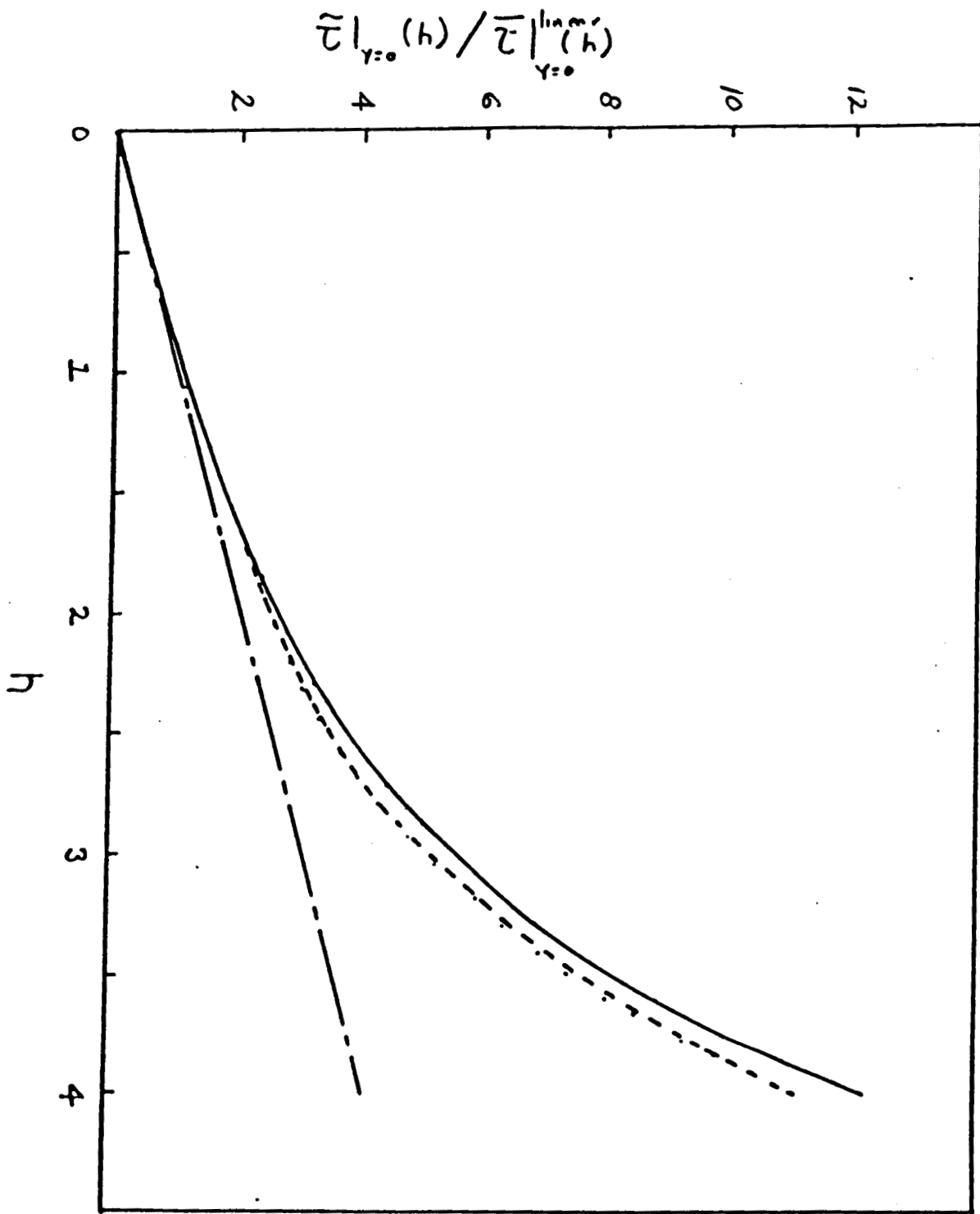


Figure 10a.

Disturbance amplitude variation versus h for $S_0 = 1$, normalized by the linearized results for $h = 1$, $S_0 = 1$. : minimum near $X = 18.5$; - - - : peak near $X = 13$; - . - : linear result.

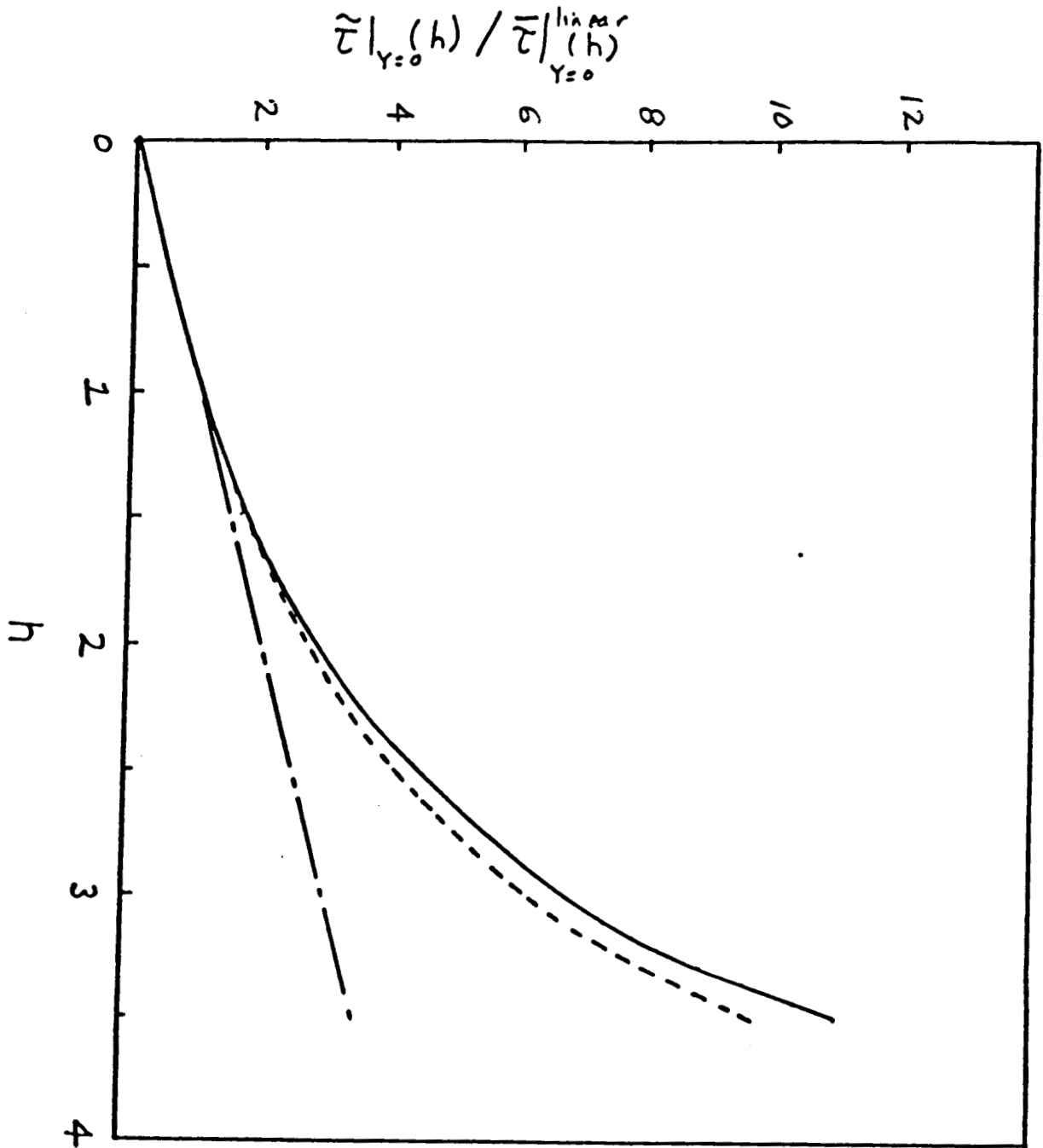


Figure 10b.

Disturbance amplitude variation versus h for $S_0 = 3$, normalized by the linearized results for $h = 1$, $S_0 = 3$. --- : minimum near $X = 9$; --- : peak near $X = 7$; - - - : linear result.